EDGE ARTICLE

Check for updates

Insights into structure–property relationships in ionic liquids using cyclic perfluoroalkylsulfonylimides†

Younes K. J. Bejaoui,[a] Frederik Philippi, [b] Hans-Georg Stammler,[c] Krzysztof Radacki,[a] Ludwig Zapf,[a] Nils Schopper,[a] Kateryna Goloviznina, [d] Kristina A. M. Maibom,[a] Roland Graf,[a] Jan A. P. Sprenger,[a] Rüdiger Bertermann,[a] Holger Braunschweig, [a] Tom Welton, [b] Nikolai V. Ignat'ev[ae] and Maik Finze [*a]

Room temperature ionic liquids of cyclic sulfonimide anions *nc*PFSI (ring size: n = 4–6) with the cations [EMIm]$^+$ (1-ethyl-3-methylimidazolium), [BMIm]$^+$ (1-butyl-3-methylimidazolium) and [BMPL]$^+$ (BMPL = 1-butyl-1-methylpyrrolidinium) have been synthesized. Their solid-state structures have been elucidated by single-crystal X-ray diffraction and their physicochemical properties (thermal behaviour and stability, dynamic viscosity and specific conductivity) have been assessed. In addition, the ion diffusion was studied by pulsed field gradient stimulated echo (PFGSTE) NMR spectroscopy. The decisive influence of the ring size of the cyclic sulfonimide anions on the physicochemical properties of the ILs has been revealed. All ILs show different properties compared to those of the non-cyclic TFSI anion. While these differences are especially distinct for ILs with the very rigid **6cPFSI** anion, the 5-membered ring anion **5cPFSI** was found to result in ILs with relatively similar properties. The difference between the properties of the TFSI anion and the cyclic sulfonimide anions has been rationalized by the rigidity (conformational lock) of the cyclic sulfonimide anions. The comparison of selected IL properties was augmented by MD simulations. These highlight the importance of π^+–π^+ interactions between pairs of [EMIm]$^+$ cations in the liquid phase. The π^+–π^+ interactions are evident for the solid state from the molecular structures of the [EMIm]$^+$-ILs with the three cyclic imide anions determined by single-crystal X-ray diffraction.

Introduction

Ionic liquids (ILs) are salts with low melting temperatures, often at or below room temperature that have attracted wide interest in academia and industry during the last decades.[1–3] The reason for this broad interest lies in their often favourable and tunable properties compared to alternative, non-ionic materials, *i.e.* traditional organic solvents. Examples of appealing properties of ILs are low dynamic viscosities, high specific conductivities, large liquid ranges, and negligible vapor pressure. The highly tuneable and versatile nature of ILs is mostly a consequence of the plethora of different combinations of anions and cations. Although major research activities have been devoted to the elucidation of nanostructures and structure–property-relationships in ILs since the early 1990s, a general concept is still missing.[4–7] However, a more profound understanding of these structure–property relationships is necessary to guide scientists in designing tailor-made ILs.

Due to the complex nature of ion interactions in ILs, many intertwining factors affecting the physicochemical properties have been identified.[6–10] Thus, the study of the influence of a specific single factor is difficult. However, the importance of ion volume[11–16] and mass[17] as well as charge delocalization (weakly coordinating nature)[18,19] of anion and cation has been studied.[20] A further properties determining factor is the conformational flexibility of the ions as a higher number of conformers increases the entropy of the liquid.[4,21–24] So, the introduction of flexible alkyl chains is a common strategy for the design of low-melting ILs, *e.g.* in 1-alkyl-3-methylimidazolium ions.[10,25,26] However, a longer alkyl chain results in higher ion mass and size as well as increased dispersion interactions, which all have the opposite effect.

aJulius-Maximilians-Universität Würzburg, Institut für Anorganische Chemie, Institut für Nachhaltige Chemie & Katalyse mit Bor (ICB), Am Hubland, 97074 Würzburg, Germany. E-mail: maik.finze@uni-wuerzburg.de

bImperial College London, Department of Chemistry, Molecular Sciences Research Hub, White City Campus, London W12 0BZ, UK

cUniversität Bielefeld, Fakultät für Chemie, Lehrstuhl für Anorganische Chemie und Strukturchemie (ACS), Centre for Molecular Materials (CM2), Universitätsstr. 25, D-33615 Bielefeld, Germany

dSorbonne Université, CNRS, Physicochimie des Électrolytes et Nanosystèmes Interfaciaux, F-75005 Paris, France

eConsultant, Merck KGaA, 64293 Darmstadt, Germany

Another example that shows the importance of conformational flexibility is the comparison of ILs with the 1-ethyl-3-methylimidazolium cation ([EMIm]$^+$) and analogous ILs with the related 1-ethyl-2,3-dimethylimidazolium cation ([EMMIm]$^+$). Although the [EMMIm]$^+$ cation suppresses hydrogen bonding at the 2-position, its ILs exhibit significantly higher viscosities. This counterintuitive behaviour is rationalized by a loss in entropy due to (i) a relatively high internal rotational barrier of the ethyl group in the [EMMIm]$^+$ cation,[10,27] and (ii) a lower number of easily accessible ion–ion conformers in the [EMMIm]$^+$-IL as a consequence of the loss of the H-bond.[28–30] A third example is ILs with ammonium cations and their isostructural phosphonium analogues. Phosphonium-ILs exhibit typically significantly lower viscosities than their ammonium derivatives, which is in part attributed to the higher conformational flexibility at the larger central P atom.[31]

Studies on the influence of conformational flexibility of anions are rare.[9,21] Most likely, this is because a targeted modification of anions is less developed compared to the derivatization of cations. However, a few examples have been described in the literature. For example, a recent molecular dynamics simulation on [BMIm][PF$_6$] (BMIm = 1-butyl-3-methylimidazolium) and [BMIm][(C$_2$F$_5$)$_3$PF$_3$] ([BMIm]**FAP**) showed that the higher flexibility of the tris(pentafluoroethyl) trifluorophosphate (**FAP**) anion is one reason among others for the low dynamic viscosity of [BMIm][(C$_2$F$_5$)$_3$PF$_3$] compared to its [PF$_6$]$^-$ counterpart.[32]

The bis(trifluoromethylsulfonyl)imide anion [(N(SO$_2$CF$_3$)$_2$]$^-$, **TFSI**)[33] represents one of the most widely studied anions in IL research.[4,34–37] It leads to low melting, low viscous and thermally robust ILs with many organic cations.[4,38] In addition, the **TFSI** anion is chemically and electrochemically very robust. As a consequence of this combination of beneficial properties, **TFSI**-ILs are among the most widely studied ILs in battery technology.[3,34,39–44] The **TFSI** anion exists in a *trans* and a *cis* conformation. According to experimental and theoretical studies, the *trans* conformer is slightly more stable than the *cis* form (Fig. 1, $\Delta H^\circ_{cis/trans} = 3 - 5$ kJ mol^{-1}) and the transition states for the interconversion of both conformers are of low energy (7–24 kJ mol^{-1}).[4] The high degree of conformational flexibility translates into a high ion mobility in and low viscosity of **TFSI**-ILs.[9,45,46]

In contrast to the **TFSI** anion, the related *cyclo*-hexafluoropropane-1,3-bis(sulfonyl)imide anion (**6cPFSI**, Fig. 1)[47] is locked in the *cis* configuration. The reduced conformational flexibility of the **6cPFSI** anion compared to the **TFSI** anion is, for example, reflected by higher melting points of [BMIm]**6cPFSI** (28 °C) compared to [BMIm]**TFSI** (−4 °C)[48] and of [*n*BuPPh$_3$]**6cPFSI** (119 °C) compared to [*n*BuPPh$_3$]**TFSI** (89 °C).[49] Similarly, the higher dynamic viscosity of [BMIm]**6cPFSI** (239 mPa s at 20 °C)[48] than of [BMIm]**TFSI** (62.3 mPa s at 20 °C)[48] has been attributed to the more rigid structure of the cyclic anion.[4] The dynamic viscosity of the [BMIm]$^+$-IL of the bis(pentafluoroethylsulfonyl)imide anion ([N(SO$_2$C$_2$F$_5$)$_2$]$^-$) is much lower (140 mPa s at 20 °C)[48] than the viscosity of [BMIm]**6cPFSI**. Thus, the higher molecular mass of the **6cPFSI** anion compared to the **TFSI** anion is not the reason for the lower dynamic viscosity of [BMIm]**TFSI**. Further salts of the **6cPFSI** anion with large organic cations have been described, which comprise comparably high melting points of more than 100 °C.[50–54]

In this study, ILs of the rigid *cyclo*-perfluoroalkanebis(sulfonyl)imide anions depicted in Fig. 1 with ring sizes of four ([*cyclo*-{CF$_2$(SO$_2$)$_2$N}]$^-$, **4cPFSI**),[55] five ([*cyclo*-{(CF$_2$)$_2$N}]$^-$, **5cPFSI**)[55] and six ([*cyclo*-{CF$_2$(CF$_2$)$_2$SO$_2$)$_2$N}]$^-$, **6cPFSI**)[47] with the widely applied countercations [EMIm]$^+$, [BMIm]$^+$ and [BMPL]$^+$ (BMPL = 1-butyl-1-methylpyrrolidinium) are presented and selected physicochemical properties are described.[56] Selected properties are compared to those of the respective **TFSI**-ILs. The structural features of the perfluoroalkanebis(sulfonyl)imide-ILs were elucidated by single-crystal X-ray diffraction (SC-XRD). We complement the experimental results with MD simulations which we performed for four prototypical ionic liquids.

Results and discussion

Synthesis

In contrast to salts of the **6cPFSI** anion, salts of the cyclic imides **5cPFSI** and **4cPFSI** are not commercially available. Thus, the ammonium salts [NH$_4$]**5cPFSI** and [NH$_4$]**4cPFSI** were synthesized according to literature procedures. The first step is the electrochemical fluorination (ECF) according to the Simons process to give the perfluorinated disulfonylfluorides FSO$_2$-CF$_2$SO$_2$F and FSO$_2$(CF$_2$)$_2$SO$_2$F,[57] which are reacted with ammonia to give [NH$_4$]**4cPFSI** and [NH$_4$]**5cPFSI**,[55,56] respectively (Scheme 1). Treatment of the ammonium salts with aqueous KOH provides access to the corresponding potassium salts of the anions **5cPFSI** and **4cPFSI**.
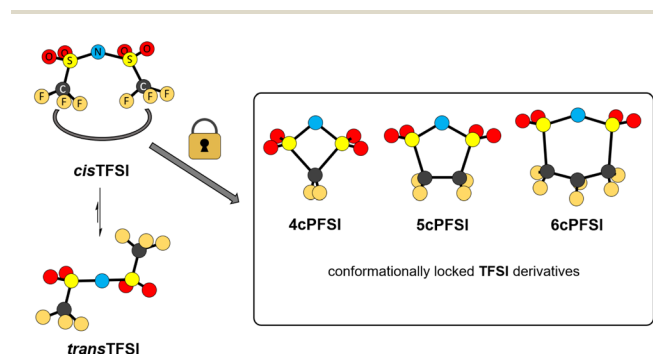

Fig. 1 Conformational interconversion of the TFSI anion and conformationally locked *cyclo*-perfluoroalkanebis(sulfonyl)imide anions.

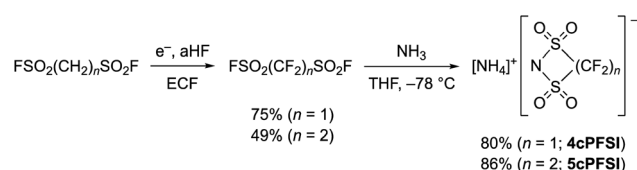Scheme 1 Electrochemical fluorination (ECF) of FSO$_2$(CH$_2$)$_n$SO$_2$F (n = 1, 2)[57] and cyclization to result in [NH$_4$]4cPFSI and [NH$_4$]5cPFSI.[55,56]

These ammonium and potassium salts were used for metathesis in water to give the corresponding IL with [EMIm]⁺, [BMIm]⁺ and [BMPL]⁺ as countercations (Fig. 2). The corresponding **6cPFSI** salts were obtained similarly using an aqueous solution of *cyclo*-hexafluoropropane-1,3-bis(sulfonyl)imide[47] (Fig. 2). All ILs were obtained as colourless to pale yellow liquids from the reaction mixtures except for [EMIm]**6cPFSI**, which precipitated as colourless solid from the aqueous mixture and was isolated by filtration. The RTILs were typically phase separated from the aqueous phase.

Alternatively, extraction with CH_2Cl_2 can be used. The ILs were washed several times with double distilled water and subsequently dried under fine vacuum. The purity of the ILs was ensured by elemental analysis, NMR spectroscopy, Karl Fischer titration (<50 ppm H_2O) and cyclic voltammetry (*vide infra*). Most likely, the repeated washing of the liquid salts (59–89%) is the reason for the relatively low yields compared to solid [EMIm]**6cPFSI** (98%).

The absence of chloride ions in the washing phase of the ILs with the cyclic imide anions **5cPFSI** and **6cPFSI** was confirmed by addition of a concentrated aqueous $AgNO_3$ solution. For the **4cPFSI**-ILs the silver nitrate test was not feasible. All three **4cPFSI**-ILs studied herein revealed some solubility in water and they formed salts after addition of aqueous silver nitrate of the complex anion $[Ag(\mathbf{4cPFSI})_2]^-$ that crystallized from the aqueous mother liquors (Fig. 3). Single crystals of [EMIm][Ag(**4cPFSI**)₂], [BMIm][Ag(**4cPFSI**)₂] and [BMPL][Ag(**4cPFSI**)₂] were studied by SC-XRD (Fig. 3). So far, we have not optimized the syntheses of the complex salts and thus, no yields are given.

The Ag atom of the $[Ag(\mathbf{4cPFSI})_2]^-$ anion in the [EMIm]⁺ salt is located on an inversion center and hence, the N···Ag···N unit is linear (Fig. 3, Table S6 in the ESI†). In the [BMIm]⁺ salt the N···Ag···N unit is almost linear (178.7°) whereas in the [BMPL]⁺ salt it is slightly bent (166.7°). The Ag···N distances of the
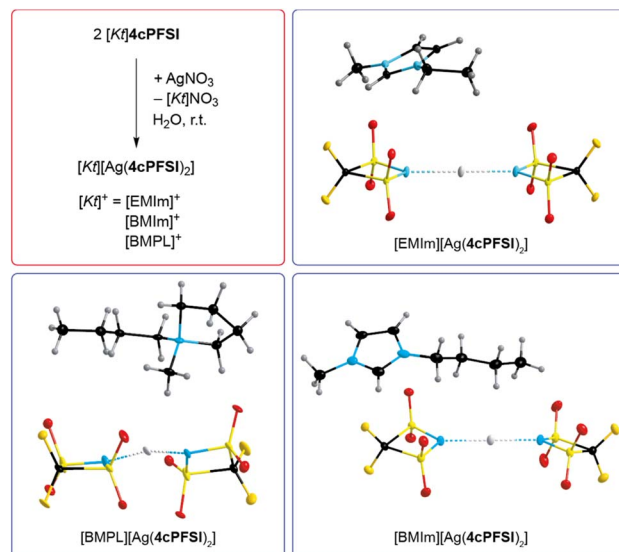

Fig. 3 Synthesis of [Kt][Ag(**4cPFSI**)₂] ([Kt]⁺ = [EMIm]⁺, [BMIm]⁺ and [BMPL]⁺) starting from the wash phase of the respective IL after addition of aqueous silver nitrate. Ion pairs of [Kt][Ag(**4cPFSI**)₂] in the crystal structure (thermal ellipsoids are set at 25% ([Kt]⁺ = [EMIm]⁺) or 50% probability ([Kt]⁺ = [BMIm]⁺ and [BMPL]⁺), H atoms are shown with arbitrary radii, disorder of the cation in [EMIm][Ag(**4cPFSI**)₂] and of both ions in [BMPL][Ag(**4cPFSI**)₂] is omitted for clarity).

anions are similar in all three structures with 214.46(12) pm in [EMIm][Ag(**4cPFSI**)₂], 215.2(6) and 214.4(6) pm in [BMIm][Ag(**4cPFSI**)₂] and 213.7(3) and 213.8(3) pm in [BMPL][Ag(**4cPFSI**)₂]. The related $[Ag(\mathbf{TFSI})_2]^-$ anion is unknown but the complex salt $[Ag(NCCH_3)_4]_2[Ag(\mathbf{TFSI})_3]$ with the dianion $[Ag(\mathbf{TFSI})_3]^{2-}$ has been structurally characterized.[58] Attempted crystallization of salts of the monoanionic silver(I) complex
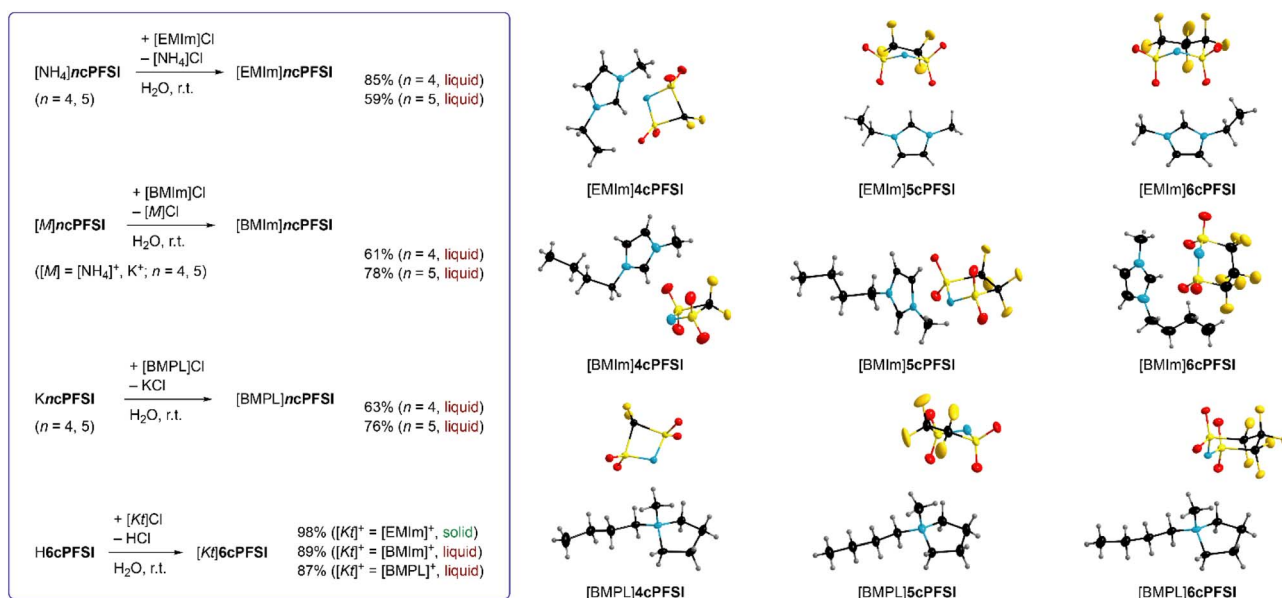

Fig. 2 Synthesis of *cyclo*-perfluoroalkylbis(sulfonyl)imide-ILs *via* metathesis in water and ion pairs of the ILs in the crystal structure (thermal ellipsoids are set at 50% ([BMPL]**5cPFSI**: 20%) probability, H-atoms are depicted with arbitrary radii and any disorder omitted for clarity).

$[Ag(\textbf{TFSI})_2]^-$ remained unsuccessful, so far. For example, crystals of $^3_\infty\{Ag\textbf{TFSI}\}$ were obtained from a mixture of [EMIm]**TFSI** and Ag**TFSI** in dichloromethane.[59] Other bis(sulfonyl)imide anions such as $[N(SO_2F)_2]^-$ and $[N(SO_2CH_3)_2]^-$ led to linear, two-coordinate argentate complexes, *e.g.* in $[Ag(NCCH_3)_2][Ag\{N(SO_2F)_2\}_2]$[60] and $[Ag(NCCH_3)_4][Ag\{N(SO_2CH_3)_2\}_2]$.[61]

Crystal structures

The crystal structures of all ILs with the three cyclic imide anions **4cPFSI**, **5cPFSI** and **6cPFSI** in combination with the countercations [EMIm]⁺, [BMIm]⁺ and [BMPL]⁺ were determined (Fig. 2). In addition, the crystal structure of [BMIm] *cis*TFSI was redetermined.[62] The single-crystal X-ray diffraction studies provide a detailed insight into the arrangement and interactions of the ions in the solid state. Ion–ion interactions in the solid are known to often correlate to ion–ion interactions in the corresponding liquid phase,[63–68] *i.e.* in recent years, theories of quasi- and pseudo-lattices have been established, which view the liquid phase as a collapsed crystal.[69–72] Crystals of salts with melting points below room temperature (*vide infra*) were grown by manual *in situ* cryocrystallization. Selected bond parameters of the cyclic imide anions **4cPFSI**, **5cPFSI** and **6cPFSI** as well as the **TFSI** anion are collected in Table 1.

The symmetry of the **4cPFSI** anion in its [EMIm]⁺ salt is close to C_{2v}, which nicely agrees with the calculated structure (Table 1). In the [BMIm]⁺ and [BMPL]⁺ salt, the N atom is significantly bent out of the S–C–S plane, which leads to a reduced C_s symmetry. A similar deviation from C_{2v} symmetry of the **4cPFSI** anion was reported for [NH₄]**4cPFSI**[73] and K**4cPFSI**.[55] The **5cPFSI** anion adopts a half-chair conformation (C_1 symmetry) in the three crystal structures and in Rb**5cPFSI** that was studied,

earlier.[55] The **6cPFSI** anion reveals an almost ideal chair conformation close to C_s symmetry in the three crystal structures. The same conformation was reported for salts of the **6cPFSI** anion with inorganic and organic cations, previously.[49,53,54,74–76] So, the **5cPFSI** anion has the lowest symmetry of the three related imide anions.

The S–N–S angle increases with increasing ring size from *ca.* 101° in **4cPFSI** to approximately 114° in **5cPFSI** and to *ca.* 120° in **6cPFSI** (Table 1). The latter angle is still slightly smaller than the S–N–S angle in the *cis*- and *trans*-conformer of the parent **TFSI** anion with *ca.* 125–127° (Table 1). The significantly smaller S–N–S angle, especially in **4cPFSI**, reflects a different electronic situation at nitrogen, which is also indicated by the ready formation of the argentate complex $[Ag(\textbf{4cPFSI})_2]^-$ (Fig. 3). Similar to the S–N–S angle, the N–S–C angles increase with increasing ring size. The distances $d(N–S)$, $d(S–C)$ and $d(S=O)$ decrease in the row **4cPFSI**, **5cPFSI** and **6cPFSI**. However, the differences are small and thus, in most cases not significant but in line with calculated bond distances. The bonding parameters of the six-membered ring derivative **6cPFSI** are closest to those of the *cis*TFSI anion (Table 1).

The van der Waals volume of the imide anions was assessed using the program packages Olex2 (ref. 77) and Platon[78–80] (Table 2). Both methods gave very similar volumes. The van der Waals volume increases in the order **4cPFSI**, **5cPFSI** and **6cPFSI**. The volumes of the *cis*- and *trans*-conformers of the non-cyclic **TFSI** anion do not differ. This result agrees with earlier studies that resulted in very similar volumes of both conformers, as well.[81,82] The volume of the **TFSI** anion is a little smaller than the volume of **6cPFSI** but significantly larger than $V_{m(vdW)}^-$ of **5cPFSI**. The van der Waals volume linearly increases with the molecular mass (Fig. S41 in the ESI†).
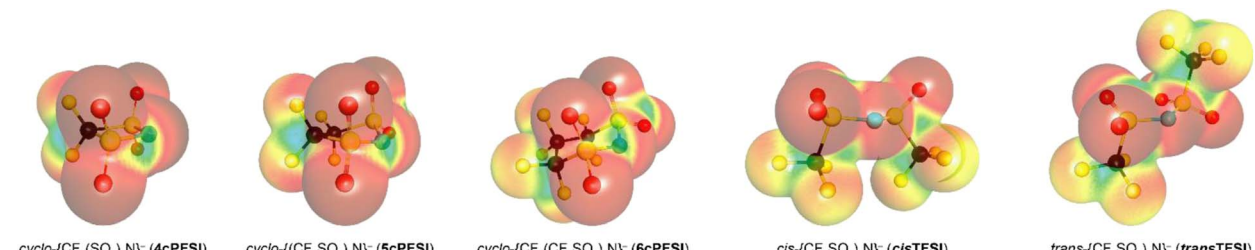
Table 1 Selected bond parameters of **4cPFSI**, **5cPFSI**,[a] and **6PFSI** in the crystal structures of their [EMIm]⁺, [BMIm]⁺, and [BMPL]⁺ salts and of the TFSI anion in [BMIm]*cis*TFSI and [BMPL]*trans*TFSI and calculated bond parameters[b]

IL		Sym.[c]	$d(N–S)$[d]	$d(S–C)$[d]	$d(S=O)$[d]	∡(S–N–S)	∡(N–S–C)	φ(S–N–S–C)[e]
[EMIm]**4cPFSI**		C_1 (C_{2v})	1.605(2)	1.855(8)	1.439(2)	101.22(8)	87.37(7)/87.46(8)	1.64(9)/−1.64(9)
[BMIm]**4cPFSI**[f]		C_1 (C_s)	1.602(2)	1.851(2)	1.435(2)	101.10(9)	87.55(8)/87.13(8)	4.83(9)/−4.81(9)
[BMPL]**4cPFSI**		C_1 (C_s)	1.611(2)	1.859(3)	1.437(2)	100.97(11)	86.83(10)/87.31(10)	8.12(11)/−8.09(11)
PBE0/def2-TZVPP		C_{2v}	1.599	1.856	1.440	101.8	87.1	0
[EMIm]**5cPFSI**		C_1	1.587(2)	1.853(2)	1.433(3)	112.9(1)	96.13(8)/98.81(8)	45.8(1)/−34.3(1)
[BMIm]**5cPFSI**	Anion 1[g]	C_1	1.588(3)	1.856(3)	1.429(2)	114.03(15)	97.03(12)/99.41(12)	25.9(2)/−41.7(2)
[BMIm]**5cPFSI**	Anion 2[g]	C_1	1.591(2)	1.854(3)	1.429(2)	113.00(15)	96.89(12)/99.02(12)	33.8(2)/−44.7(2)
PBE0/def2-TZVPP		C_1	1.584	1.866	1.436	115.1	96.3/98.7	29.5/−42.7
[EMIm]**6cPFSI**	Anion 1[g]	C_1 (C_s)	1.583(2)	1.837(3)	1.430(2)	120.29(10)	101.09(9)/101.77(9)	64.21(13)/−64.47(13)
[EMIm]**6cPFSI**	Anion 2[g]	C_1 (C_s)	1.582(2)	1.842(3)	1.430(2)	120.33(10)	101.44(9)/101.45(9)	63.70(13)/−65.03(12)
[BMIm]**6cPFSI**	Anion 1[g]	C_1 (C_s)	1.584(7)	1.841(9)	1.425(6)	119.7(4)	100.9(4)/102.0(4)	64.2(5)/−65.2(5)
[BMIm]**6cPFSI**	Anion 2[g]	C_1 (C_s)	1.585(5)	1.839(9)	1.425(6)	119.9(3)	100.9(3)/101.9(3)	63.9(5)/−64.6(5)
[BMPL]**6cPFSI**		C_1 (C_s)	158.6(3)	184.5(4)	142.9(4)	119.7(2)	100.66(14)/100.71(14)	66.5(2)/−66.2(2)
PBE0/def2-TZVPP		C_s	1.579	1.856	1.433	122.2	101.0/101.0	64.1/−64.1
[BMIm]*cis*TFSI	Anion 1[g]	C_1	1.575(5)	1.836(7)	1.430(5)	125.9(3)	100.3(3)/106.7(3)	117.6(4)/−82.5(4)
[BMIm]*cis*TFSI	Anion 2[g]	C_1	1.578(6)	1.842(9)	1.429(5)	126.9(4)	101.8(3)/104.5(4)	116.2(5)/−99.8(5)
PBE0/def2-TZVPP		C_1	1.571	1.853	1.434	127.9	98.7/104.6	88.5/−131.9
[BMPL]*trans*TFSI[64]		C_1	1.583(3)	1.839(4)	1.431(3)	124.6(2)	104.8(2)/104.4(2)	85.5(3)/89.3(3)
PBE0/def2-TZVPP		C_2	1.574	1.853	1.433	127.2	102.2	94.0

[a] [BMPL]**5cPFSI** was not considered due to disorder of the anion. [b] Bond lengths in Å and angles in °. [c] Symmetry of the anion; values in brackets indicate close higher symmetry. [d] Mean values where applicable. [e] Dihedral angle. [f] The disordered anion was not considered. [g] Two independent formula units in the unit cell.

Table 2 Selected structural and crystallographic data of the ILs of **4cPFSI**, **5cPFSI**, **6cPFSI**, *cis*TFSI, and *trans*TFSI including anion volume ($V_{m(vdW)}^-$) and mass (M_{anion}) and electrostatic surface potential (ESP) plots^a of the bis(perfluoroalkylsulfonyl)imide anions

cyclo-{CF$_2$(SO$_2$)$_2$N}$^-$ (**4cPFSI**)   cyclo-{(CF$_2$SO$_2$)$_2$N}$^-$ (**5cPFSI**)   cyclo-{CF$_2$(CF$_2$SO$_2$)$_2$N}$^-$ (**6cPFSI**)   cis-{CF$_3$SO$_2$)$_2$N}$^-$ (*cis*TFSI)   trans-{CF$_3$SO$_2$)$_2$N}$^-$ (*trans*TFSI)

Anion	M_{anion} [g mol^{-1}]	Cation	T [°C]	s.g.^{b}	Z	Z'	V_{cell} [Å^3]	$V_m{}^c$ [Å^3]	P(Platon)^d [%]	$V_{m(vdW)}$(Platon)^e [Å^3]	$V_{m(vdW)}^-$ (Platon)^f [Å^3]	$V_{m(vdW)}^-$ (Olex2)^g [Å^3]	$V_{m(vdW)}^+$ (Olex2)^g [Å^3]
4cPFSI	192.13	[EMIm]$^+$	100	$P\bar{1}$	2	1	603.04(3)	302	70.9	214	104	103	104
		[BMIm]$^+$	100	$Pbca$	16	2	5725.43(8)	358	68.1	244	102	103	133
		[BMPL]$^+$	100	$P2_12_12_1$	4	1	1484.43(2)	371	69.9	259	101	104	144
5cPFSI	242.14	[EMIm]$^+$	100	$P\bar{1}$	2	1	692.05(7)	346	69.0	239	129	128	104
		[BMIm]$^+$	100	$P\bar{1}$	4	2	1568.45(3)	392	68.9	270	128	128	133
		[BMPL]$^+$	100	$P2_1/n$	4	1	1663.88(6)	416	67.8	282	124	128	143
6cPFSI	292.15	[EMIm]$^+$	100	$P\bar{1}$	4	2	1542.43(6)	386	69.4	268	158	154	104
		[BMIm]$^+$	100	$Pca2_1$	8	2	3507.12(10)	438	67.4	295	153	153	133
		[BMPL]$^+$	100	$P\bar{1}$	2	1	882.98(2)	441	70.5	311	153	154	144
*cis*TFSI	280.14	[BMIm]$^+$	100	$P2_1/n$	8	2	3471.91(5)	434	66.7	289	147	148	134
*cis*TFSI		[HexPyrr]$^+$	125	$P\bar{1}$	4	2	1966.0(6)	492	64.7	318	147	148	159
*trans*TFSI		[BMPL]$^+$	130	$P2_12_12_1$	4	1	1811.1(4)	453	67.4	305	147	148	145

^{a} Calculated at the PBE0/def2-TZVPP level of theory. ^{b} s.g. = space group. ^{c} $V_m = V_{cell} \times Z^{-1}$. ^{d} P = packing index.^{78,79} ^{e} van der Waals volume of one formula unit obtained with the Platon program package.$^{78-80}$ ^{f} $V_{m(vdW)}^-$(Platon) = $V_{m(vdW)}$(Platon) − $V_{m(vdW)}^+$; $V_{m(vdW)}^+$([EMIm]$^+$) = 110 ± 1.4 Å^3, $V_{m(vdW)}^+$([BMIm]$^+$) = 142 ± 1.5 Å^3, $V_{m(vdW)}^+$([BMPL]$^+$) = 158 ± 7 Å^3, 171 ± 0.7 Å^3.^{83} ^{g} van der Waals volume calculated from the crystallographic data using the Olex2 program.^{77}

Hirshfeld surface analyses,$^{84-88}$ which is a well-established tool for the interpretation of intermolecular interactions in crystal structures in general, and of organic salts and ionic liquids in particular,^{49,54,89,90} have been performed to study the noncovalent interionic interactions in the crystals. The program CrystalExplorer17 was used for the analysis.^{91,92}

The [EMIm]$^+$ salts of the three cyclic anions **4cPFSI**, **5cPFSI** and **6cPFSI** crystallize in the triclinic space group $P\bar{1}$ (Table S5 in the ESI†). In contrast, [EMIm]*cis*TFSI crystallizes in the non-centrosymmetric orthorhombic space group $Pca2_1$.^{63} In all four structures, the anions and cations are interlinked via S= O···H, N···H and F···H hydrogen bonds,^{30,93} as exemplified by the Hirshfeld surfaces in Fig. 4 and evident from the Hirshfeld surface contributions (Table S7 in the ESI†) and the fingerprint plots$^{84-88,92}$ depicted in Fig. S44–S48 in the ESI.† The Hirshfeld analyses show that the S=O···H interactions are the shortest cation–anion interactions in all crystals, which parallels earlier observations on crystal structures of salts of imide anions, e.g. **TFSI**,^{49,63,90} **6cPFSI**,^{49} and [N(SO$_2$CH$_3$)$_2$]$^-$ ([NMes$_2$]$^-$).^{90} The H-bonded motifs are complex and include bi- and trifurcated interactions. The most pronounced H-bonds are found for the H atoms of the central imidazolium ring, which are the most acidic ones. However, further H-bonds are present for the alkyl chains.

In the crystals of the [EMIm]$^+$ salts of the three cyclic anions **4cPFSI**, **5cPFSI** and **6cPFSI** the imidazolium rings of two neighbouring [EMIm]$^+$ cations reveal antiparallel anion-templated π^+–π^+ stacking as depicted in Fig. 5. The π^+–π^+ stacking is evident from the pattern of red and blue triangles in the same region of the shape index placed onto the Hirshfeld surface of the [EMIm]$^+$ cation.^{84} It is also obvious from the plots of the surrounding of the anions **4cPFSI**, **5cPFSI** and **6cPFSI** by the cations in Fig. 4. In all three salts the imidazolium planes are parallel to each other as a result of crystallographic symmetry. The centroid–centroid distances (d_π) are similar for the three analogues and they range from 3.6874(19) to 4.0454(19) Å. The antiparallel aligned [EMIm]$^+$ cations are shifted from an ideal stacked position and hence, the distances between the planes (d_{plane}) of 3.243(4) to 3.447(3) Å are shorter than d_π (Fig. 4). The occurrence of π^+–π^+ stacking between imidazolium rings has been observed for different imidazolium cations by SC-XRD.$^{94-98}$ In most cases, small anions that efficiently compensate for the positive charge are present and the imidazolium cations are typically arranged in an antiparallel fashion. Furthermore, imidazolium cations with small, sterically non-demanding substituents, especially hydrogen and methyl, tend to form anion-templated π^+–π^+ dimers. So, π^+–π^+ stacking of [EMIm]$^+$ cations has been rarely observed in the solid state. One of the rare examples is the crystal structure of [EMIm]Cl.^{95} The shortest distances in the crystal structure of [EMIm]Cl are 3.791(17) Å for the ring–ring distance (d_π) and 3.60(3) Å for d_{plane}. Both values are similar to those found for the
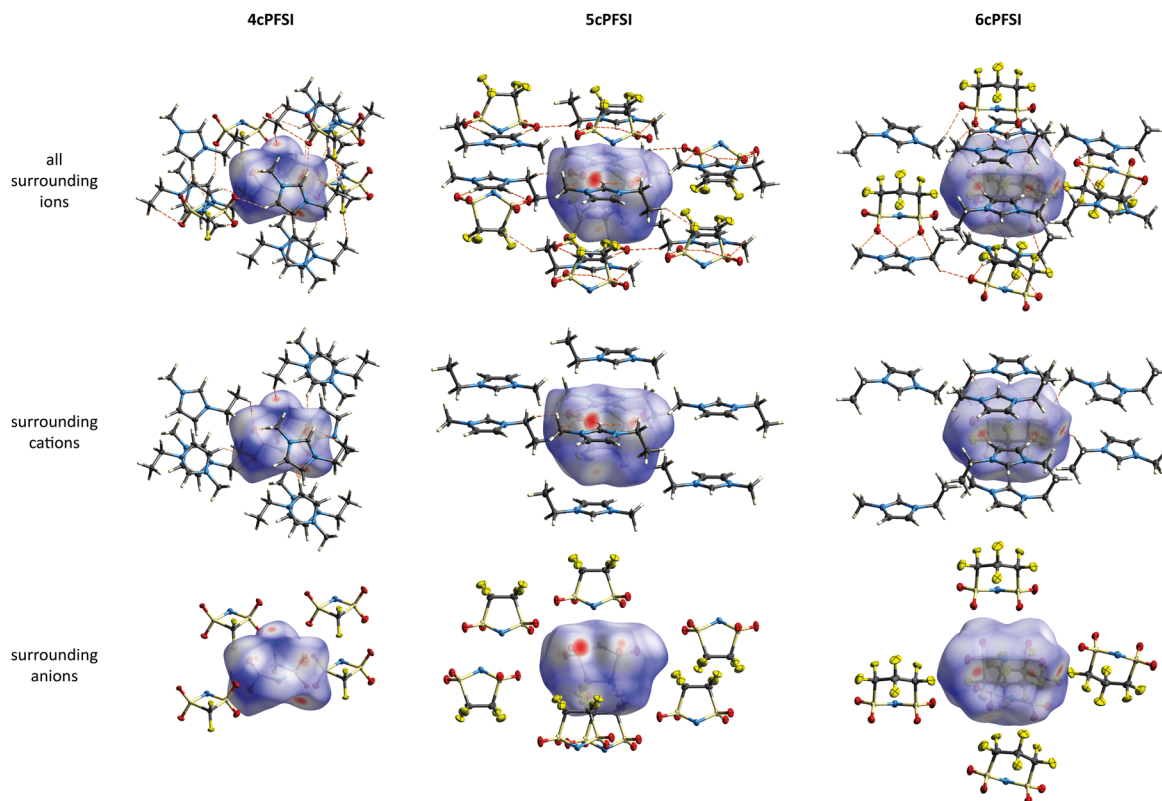
Fig. 4 Environments of the cyclic imide anions **4cPFSI**, **5cPFSI** and **6cPFSI** in the crystal structures of their [EMIm]$^+$ salts. d_{norm} mapped onto the Hirshfeld surfaces of the respective central imide anion (thermal ellipsoids set at 50% probability, H-atoms are shown with arbitrary radii).

related salt [EMMIm]Cl[98] and for [EMIm]n**cPFSI** (n = 4–6) in the present study.

The nature of π^+–π^+ stacking, in general, and for imidazolium cations, in particular, has been the subject of theoretical studies.[94,99–105] In these studies it has been pointed out that smaller anions that form comparably strong hydrogen bonds foster the occurrence of π^+–π^+ stacking while efficient anion–π^+ interactions that tend to increase with increasing anion size compete with cation–cation π^+–π^+ stacking.[99–102] Although the binding energy between the imidazolium rings is rather small, π^+–π^+ interactions are predicted to significantly influence the physicochemical properties of imidazolium ILs, *e.g.* viscosity[102] and interactions with surfaces of electrodes.[103]

In contrast to the structures of the three cyclic imide ILs [EMIm]n**cPFSI** (n = 4–6), in the crystal structure of [EMIm] *cis*TFSI no π^+–π^+ stacking is found.[63] Thus, the occurrence of π^+–π^+ stacking interactions in the [EMIm]$^+$ salts of the three cyclic imide anions and the absence of such interactions in the crystal of the *cis*TFSI salt points towards significant differences of the properties of the closely related anions and their salts (*vide infra*). However, although the missing π^+–π^+ stacking interactions in [EMIm]*cis*TFSI highlight a significant difference, the plots of the three-dimensional packing diagrams in Fig. 6 of [EMIm]**5cPFSI** and [EMIm]*cis*TFSI show the similarity of the packing, in general. The anions and cations form stacks in the crystals and the anion–cation arrangement can be distinguished into more ionic and more non-ionic domains.

The MD simulations demonstrate that the π^+–π^+ stacking observed in the experimental crystal structure is also present in the bulk liquid [EMIm]**5cPFSI** (Fig. 5). Specifically, a comparable degree of stacking was observed for the two ionic liquids [EMIm]**TFSI** and [EMIm]**5cPFSI** (Fig. S21–S23 in the ESI†).

The crystal structures of [BMIm]n**cPFSI** (n = 4–6) and [BMIm] *cis*TFSI show similar interactions and distances between anions and cations, and anions and anions, as their [EMIm]$^+$ counterparts as exemplified for [BMIm]**5cPFSI** in Fig. 7. However, in contrast to the [EMIm]$^+$ salts of **4cPFSI**, **5cPFSI** and **6cPFSI**, the respective [BMIm]$^+$ salts do not show any π^+–π^+ interactions in the crystal. Most likely, the sterically more demanding *n*-butyl groups, which are aligned next to each other (Fig. 7), prevent the stacking between the imidazolium rings. This observation is in line with earlier experimental observations, *e.g.* for picrate ILs π^+–π^+ stacking was found for the [MMIm]$^+$ salt but not for the related [PMIm]$^+$ salt (MMIm = 1,3-dimethylimidazolium; PMIm = 1-propyl-3-methylimidazolium).[96]

The interactions between the fluorinated imide anions are based on weak F···F contacts. These interactions are evident from the Hirshfeld surface contributions in Table S7 in the ESI† and illustrated in the 2D-fingerprint plots of the anions in Fig. S44, S46 and S48 in the ESI.† In addition, they are shown for the structures of the [EMIm]$^+$-ILs in Fig. 4 in the anion representations (bottom figures). The orientations of the anions **5cPFSI** and the *cis*TFSI in Fig. 6 show the close proximity of the fluorine atoms of different anions, which is indicative for weak F···F interactions. These F···F interactions range in [EMIm]
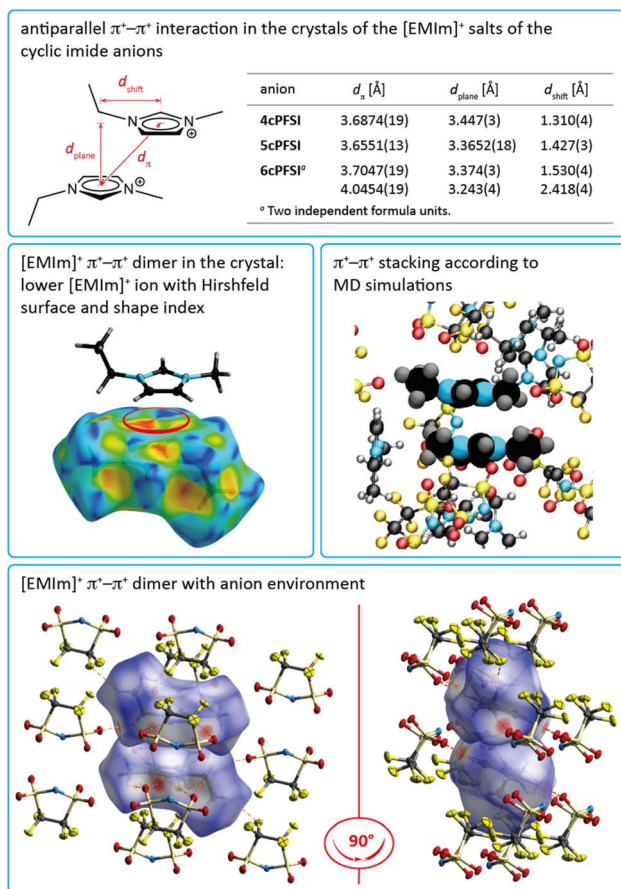
Fig. 5 Antiparallel displaced $\pi^+-\pi^+$ stacking of [EMIm]$^+$ cations in the crystal of [EMIm]$^+$ salts with *n*c**PFSI** (*n* = 4–6) counterions (top), Hirshfeld surface with shape index of an [EMIm]$^+$ cation in [EMIm] **5cPFSI** (middle, left), sketch of two [EMIm]$^+$ cations showing the π^+- π^+ stacking according to MD simulations (middle, right) and two different views of a $\pi^+-\pi^+$ [EMIm]$^+$ dimer with Hirshfeld surfaces and surrounding **5cPFSI** anions in the crystal of [EMIm]**5cPFSI** (bottom).

Fig. 6 Three-dimensional packing diagram with unit cell of [EMIm] **5cPFSI** (top) and [EMIm]*cis***TFSI** (bottom)[63] (all atoms are depicted with arbitrary radii).

5cPFSI from 2.85 to 3.57 Å. The importance of F⋯F interactions decreases with decreasing number of fluorine atoms per cyclic imide anion as shown by the Hirshfeld surface contributions in Table S7 in the ESI† and the 2D fingerprint plots in Fig. S44, S46 and S48 in the ESI.† For [BMPL]**5cPFSI** and [BMPL]**4cPFSI** no F⋯F interactions are present, at all.

Pronounced anion–anion close contacts were also observed in the MD simulations of the bulk ionic liquid [EMIm]**5cPFSI**. Fig. 8 shows the atom-resolved spatial distribution function for the anion surrounded by other anions. Fluorine–fluorine interactions dominate in these first shell contacts, see Fig. 8 for a snapshot from the simulation. We identified four prevalent mutual orientations, see ESI† for more details.

The **TFSI** anion was found to easily adopt the *cis* or the *trans* conformation in crystals of imidazolium salts, *i.e.* [EMIm] *cis***TFSI**,[63] [EMIm]*trans***TFSI**[62] and [BMIm]*cis***TFSI**.[62] Most likely, the occurrence of the *cis* conformation is due to comparably strong H-bonds between the **TFSI** anion and the relatively acidic H atoms of the central imidazolium rings that force the **TFSI** anion into the enthalpically less favoured conformer. In
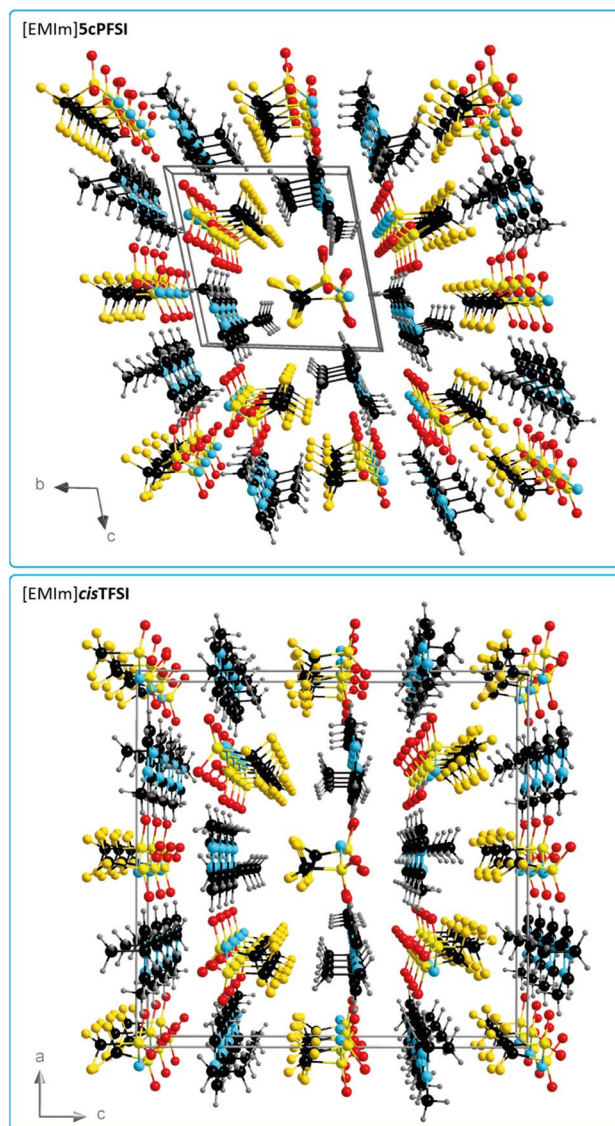
general, the H-bonded motifs with bi- and trifurcated H-bonds of the *cis***TFSI** anion in its [EMIm]$^+$ and [BMIm]$^+$ salts are very similar to those found in the respective crystal structures of [EMIm]**6cPFSI** and [BMIm]**6cPFSI**. For the [BMPL]$^+$ cation weaker H-bonds are only possible. So, it is not surprising that only the *trans***TFSI** anion was observed in the crystal of [BMPL] **TFSI**,[64] so far.

Thermal properties

The melting point and liquid range of an IL are obvious key parameters to assess its performance and potential for various applications. The thermal parameters depend on the ion mass and size, ion symmetry, the surface electron density and the ion size ratio among others. The correlation between ion rigidity/ flexibility and low melting points has been rationalized
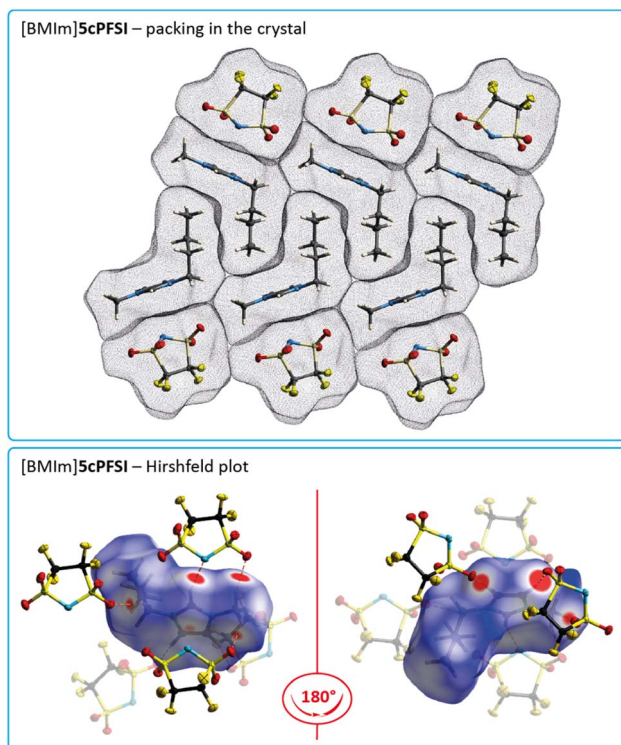
Fig. 7 Excerpt of the crystal structure of [BMIm]**5cPFSI** showing the packing of cations and anions (top) and surrounding of [BMIm]$^+$ by anions with C−H···O and C−H···N hydrogen bonding illustrated by d_{norm} mapped onto the Hirshfeld surface of [BMIm]$^+$ (bottom; thermal ellipsoids are set at 50% probability, H-atoms are depicted with arbitrary radii).
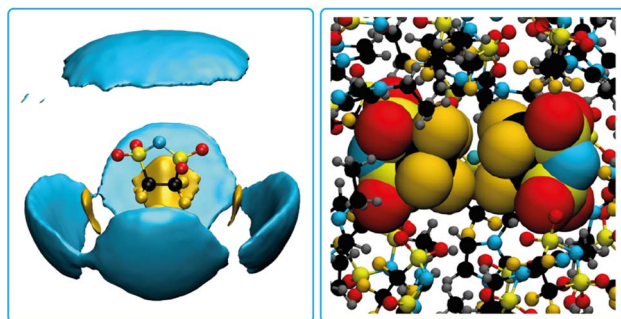

Fig. 8 Atom-resolved spatial distribution function for the **5cPFSI** anion with surrounding anions (left) and a snapshot from the MD simulation showing a pair of **5cPFSI** anions (right).

through the entropy of the liquid phase.[22] A higher number of available conformers in the liquid phase typically results in an increase of entropy leading to lower melting temperatures of the IL.[23] The influence of conformational flexibility on the thermal properties is reflected by the phase transitions of the ILs presented in this study (Table 3). Hence, it is not surprising that the **TFSI** anion, which readily switches between the *cis* and *trans* conformation, leads to ILs with very low melting points (Table 3). The respective ILs with the related cyclic imide anion **5cPFSI** have similar low melting points. In contrast, the melting points

Table 3 Thermal properties of imide ILs[a]

IL	T_{mp}[b] [°C]	T_g[c] [°C]	T_{dec}[d] [°C]
[EMIm]**4cPFSI**	27	−77	285
[EMIm]**5cPFSI**	−18[e]	−91	423
[EMIm]**6cPFSI**	67	n.o.[f]	412
[EMIm]**TFSI**	−18	−98	394
[BMIm]**4cPFSI**	16	−76	262
[BMIm]**5cPFSI**	2	−52	405
[BMIm]**6cPFSI**	28	n.o.	409
[BMIm]**TFSI**	−4	−87	404
[BMPL]**4cPFSI**	26	n.o.	251
[BMPL]**5cPFSI**	−19	−97	383
[BMPL]**6cPFSI**	20	−73	405
[BMPL]**TFSI**	−21	−88	400

[a] Temperatures are onset values (DSC). [b] T_{mp} = melting point. [c] T_g = glass transition temperature. [d] T_{dec} = decomposition temperature. [e] Melting point was determined from the *in situ* cryocrystallization experiments performed for the SC-XRD study (*vide infra*). The melting point was not observed in the DSC curve. [f] n.o. = not observed.

of the ILs of the imide anions **4cPFSI** and **6cPFSI** are significantly higher, with [EMIm]**6cPFSI** having a melting point as high as +67 °C. For the small cyclic **4cPFSI** anion, the relatively high electron density as evident from the ESP plot in Table 2 results in relatively strong cation–anion interactions. However, the argument of a high electron density does not hold for the 6-membered ring imide anion **6cPFSI** (ESP plot in Table 2). Therefore, the explanation for the high melting points of the **6cPFSI**-ILs must be different and presumably the rigidity of the **6cPFSI** anion, which favours the chair conformation, is the reason. In contrast, switching between the half-chair and the envelope conformation of the **5cPFSI** anion is accompanied by almost no change in energy (Fig. 9). Despite the aforementioned strong cation–anion interactions between [EMIm]$^+$ and the
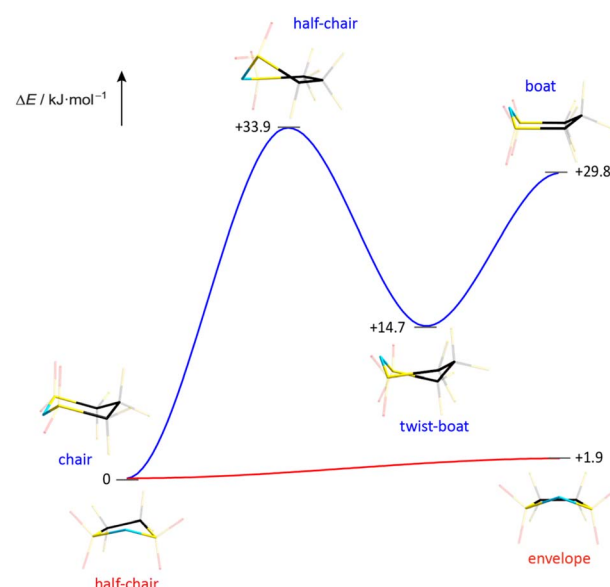

Fig. 9 Energy profile for the conformational change of the cyclic imide anions **5cPFSI** and **6cPFSI** (PBE0/def2-TZVPP).

4cPFSI anion, this small 4-membered cyclic imide anion is rigid (Fig. S37 in the ESI†), which might contribute to the comparably high melting point of 27 °C. Most of the ILs studied herein form supercooled liquids with glass transition temperatures below −50 °C (Table 3). The only exceptions are [EMIm]**6cPFSI**, [BMIm]**6cPFSI** and [BMPL]**4cPFSI** that crystallize upon cooling. So, again the rigid anion **6cPFSI** shows the strongest tendency for crystallization.

The thermal stabilities of the ILs with the cyclic imide anions **5cPFSI** and **6cPFSI** with all three countercations [EMIm]$^+$, [BMIm]$^+$ and [BMPL]$^+$ are in the range of 383–423 °C and thus, similar to the stabilities of the **TFSI** salts. Although all **4cPFSI**-ILs exhibit significantly lower decomposition temperatures than the other imide-ILs studied herein, their thermal stabilities are surprisingly high with decomposition temperatures of more than 250 °C (Table 3). Probably, the comparably low decomposition temperature is related to the ring strain of the small cyclic imide anion **4cPFSI**, which is also the reason for its relatively high sensitivity to strong Brønsted acids.[106]

Behaviour against elemental lithium

A freshly cut piece of elemental lithium was added to a small sample of the neat ionic liquid [Kt]**ncPFSI** ([Kt]$^+$ = [BMIm]$^+$, [BMPL]$^+$; n = 4–6) under an Ar atmosphere and stored at 30 °C for 24 hours. The lithium surfaces became brownish and the ionic liquids changed their colour to yellow or pale brownish. In some cases, formation of a few gas bubbles was observed. However, the ^{1}H, ^{19}F and ^{13}C NMR spectra revealed no significant changes of the ILs after storage in the presence of lithium at 30 °C and most of the ^{7}Li NMR spectra revealed the presence of a minor amount of a Li species (−1.0 to −2.5 ppm). The six ILs were heated to 70 °C for further 24 hours in the presence of lithium but no significant changes were detected neither visually nor by multinuclear NMR spectroscopy. Thus, the ILs based on the three cyclic imide anions **4cPFSI**, **5cPFSI** and **6cPFSI** are stable against lithium after initial passivation. Furthermore, we have no signs for any reaction of the three anions with elemental lithium.

Electrochemical properties

Since ionic liquids consist purely of ions this substance class of compounds is of utmost interest for various electrochemical applications, *e.g.* batteries and supercapacitors (supercaps),[2,3,43,44,107–116] and for chemical synthesis where electrochemical stability is of relevance.[117–120] Thus, their electrochemical stability is a decisive parameter and the understanding of factors that determine their key physicochemical properties is of utmost importance.

The [EMIm]$^+$-, [BMIm]$^+$- and [BMPL]$^+$-ILs with the cyclic imide anions **ncPFSI** (n = 4–6) possess large electrochemical windows of 4.2 to 5.3 V in acetonitrile (0.1 mol L^{-1}) that are similar to those of the related **TFSI**-ILs (Fig. 10 and Table 4). The smallest anion **4cPFSI** has the lowest oxidative stability for all three types of ILs. The ILs with the larger imide anions **5cPFSI**, **6cPFSI** and **TFSI** have very similar anodic limits (E_a) and do not show a clear trend with respect to oxidative stability. The
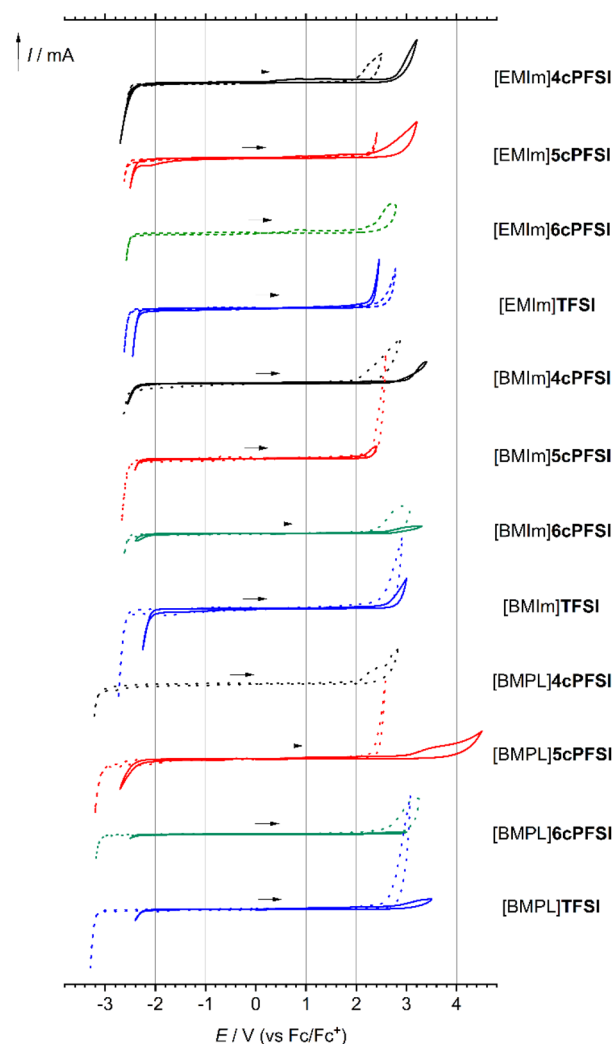

Fig. 10 Cyclic voltammograms of imide ionic liquids with the cations [EMIm]$^+$, [BMIm]$^+$ and [BMPL]$^+$ (solid line: neat IL; dashed line: solution of the IL in CH$_3$CN (0.1 mol L^{-1}) at 20 °C, scan rate: 50 mV s^{-1}, glassy carbon working electrode).

reductive stability of the ILs in CH$_3$CN is determined by the cation and thus, no dependence on the counteranion is evident.

The neat ILs reveal similarly large electrochemical windows as their solutions in CH$_3$CN (Fig. 10 and Table 4). Noticeably, [EMIm]**4cPFSI** and [BMIm]**4cPFSI** are found to provide larger electrochemical windows than the respective **TFSI**-ILs, which is in stark contrast to the behaviour of the solutions in acetonitrile. This difference may be a consequence of relatively strong ion–ion interactions in the neat ILs due to the small size and thus high electron density; see ESP plots in Table 2 and compare to the easy formation of silver(I) complexes (Fig. 3). The cyclic voltammograms of the neat RTILs in Fig. 10 show a correlation between the amperage of reduction and oxidation with the viscosity and diffusivity of the ions (*vide infra*). A higher dynamic viscosity results in a smaller current for the respective redox events.

Table 4 Electrochemical properties of bis(perfluoroalkylsulfonyl)imide-ILs at 20 °C[a]

IL	Neat IL			Solution in CH$_3$CN (0.1 mol L^{-1})		
	E_c [V]	E_a [V]	ΔE [V]	E_c [V]	E_a [V]	ΔE [V]
[EMIm]**4cPFSI**	−2.4[b]	2.8[b]	5.2[b]	−2.4	1.8	4.2
[EMIm]**5cPFSI**	−2.4	2.8	5.2	−2.5	2.2	4.7
[EMIm]**6cPFSI**	—[c]	—[c]	—[c]	−2.4	2.1	4.5
[EMIm]**TFSI**	−2.4	2.3	4.7	−2.4	2.1	4.5
[BMIm]**4cPFSI**	−2.4	2.9	5.4	−2.4	1.8	4.2
[BMIm]**5cPFSI**	−2.3	2.3	4.6	−2.5	2.5	5.0
[BMIm]**6cPFSI**	−2.1	2.5	4.6	−2.5	2.2	4.7
[BMIm]**TFSI**	−2.1	2.6	4.7	−2.5	2.4	4.9
[BMPL]**4cPFSI**	—[c]	—[c]	—[c]	−3.0	2.0	5.0
[BMPL]**5cPFSI**	−2.1	2.5	4.6	−3.0	2.3	5.3
[BMPL]**6cPFSI**	−2.2	2.8	5.0	−3.0	2.3	5.3
[BMPL]**TFSI**	−2.1	2.3	4.4	−3.1	2.5	5.6

[a] Cathodic and anodic limits E_c and E_a; electrochemical window $\Delta E = E_a - E_c$. [b] Supercooled melt. [c] Solid at 20 °C.

Viscosities and conductivities

The viscosity is a key parameter for the application of ionic liquids in materials science and a low viscosity that leads to a high conductivity is preferable, in general.[21,121–123] The viscosity of an ionic liquid is determined by a number of in part mutually influencing factors,[21,69,124] including ion volume[11–16] and mass,[17] ion–ion interactions (Coulomb interaction, hydrogen bond, *etc.*)[15,18,19,125] and conformational flexibility.[4,22–24]

For all three different types of ILs with the cations, [EMIm]$^+$, [BMIm]$^+$ and [BMPL]$^+$, the respective **TFSI**-IL possesses the lowest dynamic viscosity (Table 5 and Fig. 11). [EMIm]**6cPFSI** melts at 67 °C and does not form supercooled melts, which prevented its study by viscometry. The ILs with the [BMPL]$^+$ cation possess the highest dynamic viscosities, respectively, while η of the BMIm-ILs are in between.

The dynamic viscosities of the ILs with the cyclic imide anions **4cPFSI** and **5cPFSI** are similar for the three different countercations in the full temperature range investigated (20–80 °C; Fig. 11). For [EMIm]$^+$ and [BMPL]$^+$ the ILs with the **4cPFSI** anion are less viscous than those with the slightly larger and heavier **5cPFSI** anion whereas with the [BMIm]$^+$ cation the opposite behaviour is found (Table 5 and Fig. 11). The ILs with the non-cyclic **TFSI** anion show the lowest viscosities with all three different cations and at 20 °C, η is approximately 1.3–1.5 times higher for the ILs with **4cPFSI** and **5cPFSI** compared to the **TFSI**-ILs (Table 5). ILs with the **6cPFSI** anion reveal significantly higher viscosities than the related ILs with the smaller cyclic imide anions and the **TFSI** anion (Table 5 and Fig. 11). The large, almost equal dynamic viscosities of the ILs with the anions **4cPFSI** and **5cPFSI** and the strong increase for the analogous ILs with the **6cPFSI** anion cannot be rationalized by differences in mass or volume as these should result in a consistent trend for η for these anions. Since the delocalization of the negative charge is most effective in **6cPFSI** and least effective in **4cPFSI**, one would expect the highest fluidity for the **6cPFSI**-ILs, which is not the case. However, this might be one reason for the very similar dynamic viscosities of **4cPFSI**- and **5cPFSI**-ILs. So, the most reasonable explanation for the high dynamic viscosity of ILs with the **6cPFSI** anion is the rigidity of this cyclic imide anion (*vide supra*, Fig. 9). The low dynamic viscosities of the **TFSI**-ILs nicely agree with this argument because the **TFSI** anion is the least rigid, most flexible one in the series studied, herein.[21,23] If ion mass and size (Table 2) were the most relevant factors determining the dynamic viscosity, the **TFSI**-ILs would have properties in between those of the respective ILs with the anions **4cPFSI** and **5cPFSI**.

Similar to ILs with cyclic bis(perfluoroalkyl)imide anions, the dynamic viscosity of ILs with cyclic alkylammonium cations depends on the ring size. Typically, larger rings result in higher viscosities,[126,127] *e.g.* [BMPL]**TFSI** (85 mPa s, 298.15 K), [BMPip]**TFSI** (182 mPa s, 298.15 K; BMPip = *N*-butyl-*N*-methylpiperidinium) and [BMAzp]**TFSI** (315 mPa s, 298.15 K; BMAzp = *N*-

Table 5 Selected physical and electrochemical properties[a] of the neat bis(perfluoroalkylsulfonyl)imide-ILs at 20 °C

IL	η [mPa s]	ρ [g·cm^{-3}]	c_{IL} [mol L^{-1}]	σ [mS cm^{-1}]	D^+ [10^{-11} m^2 s^{-1}]	D^- [10^{-11} m^2 s^{-1}]	Λ_{NMR} [cm^2 S mol^{-1}]	Λ_{imp} [cm^2 S mol^{-1}]	I
[EMIm]**4cPFSI**	50.4	1.47	4.85	4.37	3.0	2.4	2.06	0.90	0.44
[EMIm]**5cPFSI**	53.0	1.53	4.33	2.84	3.0	1.9	1.87	0.66	0.35
[EMIm]**TFSI**	37.8	1.52	3.88	7.22	4.4	2.5	2.64	1.86	0.70
[BMIm]**4cPFSI**	93.8	1.38	4.16	2.00	1.4	1.2	0.99	0.48	0.48
[BMIm]**5cPFSI**	85.0	1.44	3.78	1.84	1.6	1.2	1.07	0.49	0.46
[BMIm]**6cPFSI**[b]	250.3	1.49	3.45	—	0.6	0.4	0.41	—	—
[BMIm]**TFSI**	62.0	1.44	3.43	3.11	2.2	1.6	1.96	0.91	0.46
[BMPL]**4cPFSI**[b]	129.6	1.33	3.97	—	—	—	—	—	—
[BMPL]**5cPFSI**	143.5	1.39	3.62	1.13	1.0	0.8	0.69	0.27	0.40
[BMPL]**6cPFSI**	469.2	1.50	3.45	0.34	0.3	0.2	0.21	0.10	0.48
[BMPL]**TFSI**	98.8	1.40	3.31	1.36	1.3	1.1	0.92	0.41	0.45

[a] Dynamic viscosity η; density ρ; concentration c_{IL}; diffusion coefficients of cations (D^+) and anions (D^-); specific conductivity σ measured *via* impedance spectroscopy; molar conductivities calcd by $\Lambda_{NMR} = (D^+ + D^-)N_A e^2 k^{-1} T^{-1}$ and $\Lambda_{imp} = \sigma M \rho^{-1}$; ionicity $I = \Lambda_{imp} \Lambda_{NMR}^{-1}$. [b] Solid at room temperature; η and ρ measured on a supercooled sample.
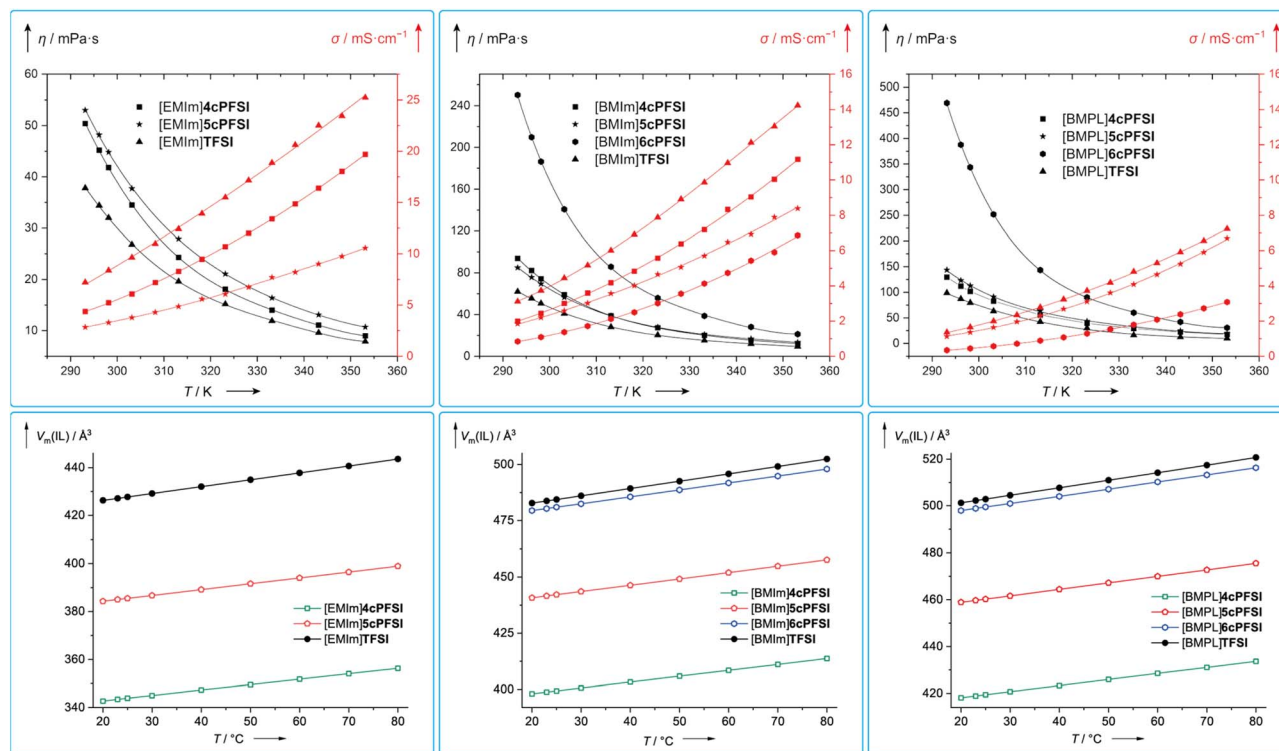
Fig. 11 Temperature dependence of the dynamic viscosities (black) and specific conductivities (red) of the neat RTILs investigated in this study (top) and their molecular volumina ($V_m(\text{IL})$) at different temperatures calculated from the densities of the neat ILs (ρ; Table S3 in the ESI†) according to $V_m(\text{IL}) = (\rho \times M_{\text{IL}}^{-1} \times N_A)^{-1}$ (M_{IL} = molecular mass of the IL; N_A = Avogadro constant; bottom).

butyl-*N*-methylazepanium).[127] A related trend was reported for the two dicyanamide-ILs [BMPL][N(CN)$_2$][128,129] (33.7–40.13 mPa s, 298.15 K)[130–132] and [BMPip][N(CN)$_2$] (119.7 mPa s, 298.15 K).[132] But the dicyanamide-IL with the smaller *N*-butyl-*N*-methylazetidinium cation [BMAze]$^+$ reveals a higher viscosity (86.7 mPa s, 298.15 K) than the respective [BMPL]$^+$-IL.[132,133] Thus, the [BMPL]$^+$ cation with the five-membered ring leads to the IL with the lowest viscosity. The general low dynamic viscosity of [BMPL]$^+$-ILs may be related to a high conformational flexibility of the five-membered ring of the [BMPL]$^+$ cation.[134] The high conformational flexibility of the [BMPL]$^+$ cation compared to the smaller [BMAze]$^+$ and the larger [BMPip]$^+$ cation also mirrors the well documented high relative entropy of the all carbon ring in cyclopentane *versus* cyclobutane and cyclohexane.[135,136]

The conductivity is another crucial bulk property of ILs. Typically, the specific conductivity increases with decreasing viscosity and generally, it correlates with the dynamic viscosity and the concentration of charge carriers.[137] The ILs studied in this contribution follow this trend, in general (Table 5 and Fig. 11). So, the **TFSI**-ILs have higher specific conductivities than their counterparts with the cyclic imide anions.

Assuming that the molecular volume of an IL ($V_m(\text{IL})$), *i.e.* the concentration (c_{IL}), correlates with its molecular mass (M_{IL}), one would expect an increase in $V_m(\text{IL})$ in the order **4cPFSI** < **5cPFSI** < **TFSI** < **6cPFSI** for a series of ILs with the same cation. The ILs with the cyclic imide anions strictly follow this trend (Fig. 11). In case of the ILs with [BMIm]**6cPFSI** and [BMIm]**TFSI** as well as

[BMPL]**6cPFSI** and [BMPL]**TFSI** the reverse behaviour is found since the **TFSI**-IL possesses a larger molecular volume than the respective **6cPFSI**-IL as calculated from the densities (ρ) of the neat ILs. These observations cannot be rationalized by the anion size as the lighter **TFSI** anion has a smaller van der Waals volume ($V_{m(\text{vdW})}^-$) compared to the heavier **6cPFSI** anion (Table 2). Thus, the **TFSI**-ILs are comparably poorly packed, revealing a relatively large free volume, which nicely agrees with the low dynamic viscosities and high specific conductivities.

Ion diffusivity

Since the macroscopic properties viscosity and conductivity are determined by the diffusion of the ions,[10,138,139] the diffusion in the neat ionic liquids was studied by pulsed field gradient stimulated echo (PFGSTE) NMR spectroscopy in the temperature range of 20–80 °C (Fig. 12 and S38–S40 in the ESI†). The diffusion coefficients nicely display the dynamic viscosities and the specific conductivities (*vide supra*).

Within the series of three [EMIm]$^+$-ILs with the anions **4cPFSI**, **5cPFSI** and **TFSI**, the **TFSI** anion possesses the highest diffusion coefficient (2.545×10^{-11} m^2 s^{-1}; Fig. 12). Its conformationally locked counterpart **5cPFSI** reveals a significantly lower (24%) diffusivity. The diffusion coefficient of the **4cPFSI** anion is in between those of the anions **TFSI** and **5cPFSI**. However, the difference in the diffusion coefficients of the three related imide anions in the [EMIm]$^+$-ILs is rather small. Interestingly, the [EMIm]$^+$ cations in [EMIm]**4cPFSI** and [EMIm]
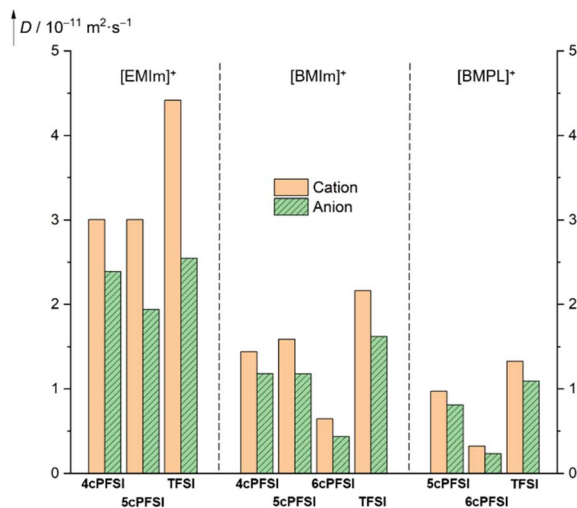
Fig. 12 Translational self diffusion coefficients of the ions of neat RTILs determined at 20 °C by PFGSTE NMR spectroscopy.

5cPFSI exhibit almost identical diffusion coefficients, while the coefficient of [EMIm]$^+$ cation in neat [EMIm]**TFSI** is 1.47 times higher. A possible explanation arises from X-ray diffraction study. The crystal structures of the [EMIm]$^+$-ILs with cyclic anions exhibit antiparallel displaced π^+–π^+-stacking (*vide infra*, Fig. 5). This greater tendency for cation–cation interactions decreases the ion mobility, which is reflected in the corresponding diffusion coefficients. These results experimentally indicate that in the liquid phase of the cyclic imide-ILs the cation–cation association by π^+–π^+-stacking evident in the crystalline state is, at least in part, retained. To establish such interactions between two cations a sufficient Coulomb stabilization provided by the counterions is needed.

The diffusion properties of the [BMIm]$^+$- and [BMPL]$^+$-RTILs reflect the effect of conformational lock of the cyclic imide anions more strongly than their [EMIm]$^+$-counterparts. The ion diffusion of the cyclic [BMIm]$^+$- and [BMPL]$^+$-ILs is significantly smaller with all cyclic imide ions compared to [BMIm]**TFSI** (Fig. 12). This strongly suggests that the reduced diffusion observed, is significantly affected by the conformational lock of the anions and not solely by other accompanying factors such as size, mass, degree of fluorination or electronic structure, since these properties differ for the three cyclic imide anions and those of the **TFSI** anion are in between.

It has been demonstrated for anions with conformational constraints that the physicochemical properties of their ILs reveal a successive reduced influence of these constraints with increasing temperature.[9] With an increasing temperature conformational barriers are overcome and the interconversion between ion conformers is more easily achieved resulting in an increased conformational flexibility.[9] Obviously the strict conformational lock present in the cyclic imide anions prevents such a behaviour, which explains that the temperature-dependent diffusion coefficients of the cyclic imide ILs do not show an analogous behaviour (Fig. S38–S40 in the ESI†).

Conclusions

Room temperature ionic liquids (RTILs) with 4- to 6-membered cyclic sulfonimide anions **4cPFSI**, **5cPFSI** and **6cPFSI** have been synthesized, which are closely related to the well-established ILs with the **TFSI** anion. The conformational lock of the cyclic sulfonimide anions is well reflected by the physicochemical properties of their ILs. Thus, the **TFSI**-ILs with the three cations [EMIm]$^+$, [BMIm]$^+$ and [BMPL]$^+$ possess lower melting points, lower viscosities and higher specific conductivities than their counterparts with the cyclic sulfonimide anions. The properties of the **5cPFSI**-ILs are closest to those of the respective **TFSI**-ILs, in general, while those of the analogous **6cPFSI**-ILs are significantly different. This is remarkable as the molecular mass and volume of the **5cPFSI** and the **6cPFSI** anion are similar (**5cPFSI**) and very similar (**6cPFSI**) to the molecular mass and size of the **TFSI** anion. So, the differences in melting point, viscosity and conductivity are mostly attributed to the conformational flexibility of the anions. The **6cPFSI** anion has comparably high barriers for the interconversion between its conformers and the **5cPFSI** anion reveals a higher conformational flexibility. In stark contrast, the **TFSI** anion easily switches between its *cis*-conformation, which resembles the cyclic sulfonimide anions, and the *trans*-conformation.

SC-XRD studies on the [EMIm]$^+$ salts of the four imide anions **TFSI** and ***n*cPFSI** (*n* = 4–6) show that the salts with the cyclic imide anions reveal distinctive π^+–π^+ interactions between two [EMIm]$^+$ cations whereas for crystalline [EMIm]**TFSI** no π^+–π^+ stacking has been observed. The π^+–π^+ interactions translate into properties of the liquid salts as demonstrated by their ion diffusion coefficients and in agreement with results of MD simulations. This observation is one of the very rare experimental examples of π^+–π^+ interactions for imidazolium cations with alkyl chains longer than methyl.

In summary, the present study shows that minor modifications of anionic IL building blocks lead to significant changes of the macroscopic properties as exemplified by a study on the ring size of cyclic anions.

Data availability

Experimental and computational data is deposited in the ESI† as well as on the Github pages given in the methodology.

Author contributions

Younes K. J. Bejaoui: conceptualisation, synthesis, spectroscopy, SC-XRD (data collection and structure solution) and interpretation, DFT calculations, writing (original draft, review and editing). Frederik Philippi: conceptualisation, MD simulations, writing (review). Hans-Georg Stammler: SC-XRD (data collection and structure solution). Krzysztof Radacki: SC-XRD (data collection and structure solution). Ludwig Zapf: cyclic voltammetry, impedance spectroscopy and SC-XRD (data collection and structure solution). Nils Schopper: cyclic voltammetry and impedance spectroscopy. Kateryna Goloviznina: force field development. Kristina A. M. Maibom: SC-XRD (data

collection and structure solution). Roland Graf: SC-XRD (data collection and structure solution). Jan A. P. Sprenger: viscometry and thermal analysis. Rüdiger Bertermann: NMR studies (PFGSTE and spectra on neat ILs). Holger Braunschweig: writing (editing). Tom Welton: conceptualisation, writing (review and editing). Nikolai V. Ignat'ev: conceptualisation, writing (original manuscript, review and editing). Maik Finze: supervision, conceptualisation, writing (original manuscript, review and editing).

Conflicts of interest

There are no conflicts to declare.

Acknowledgements

Notes and references

1 M. Kar, O. Tutusaus, D. R. MacFarlane and R. Mohtadi, *Energy Environ. Sci.*, 2019, **12**, 566–571.

2 M. Watanabe, M. L. Thomas, S. Zhang, K. Ueno, T. Yasuda and K. Dokko, *Chem. Rev.*, 2017, **117**, 7190–7239.

3 D. R. MacFarlane, M. Forsyth, P. C. Howlett, M. Kar, S. Passerini, J. M. Pringle, H. Ohno, M. Watanabe, F. Yan, W. Zheng, S. Zhang and J. Zhang, *Nat. Rev. Mater.*, 2016, **1**, 15005.

4 F. Philippi and T. Welton, *Phys. Chem. Chem. Phys.*, 2021, **23**, 6993–7021.

5 Y.-L. Wang, B. Li, S. Sarman, F. Mocci, Z.-Y. Lu, J. Yuan, A. Laaksonen and M. D. Fayer, *Chem. Rev.*, 2020, **120**, 5798–5877.

6 K. Dong, X. Liu, H. Dong, X. Zhang and S. Zhang, *Chem. Rev.*, 2017, **117**, 6636–6695.

7 W. Silva, M. Zanatta, A. S. Ferreira, M. C. Corvo and E. J. Cabrita, *Int. J. Mol. Sci.*, 2020, **21**, 7745.

8 H. Tokuda, K. Hayamizu, K. Ishii, M. A. B. H. Susan and H. Watanabe, *J. Phys. Chem. B*, 2004, **108**, 16593–16600.

9 F. Philippi, D. Pugh, D. Rauber, T. Welton and P. A. Hunt, *Chem. Sci.*, 2020, **11**, 6405–6422.

10 S. Tsuzuki, *ChemPhysChem*, 2012, **13**, 1664–1670.

11 U. P. R. M. Preiss, J. M. Slattery and I. Krossing, *Ind. Eng. Chem. Res.*, 2009, **48**, 2290–2296.

12 Y. Marcus, *J. Mol. Liq.*, 2015, **209**, 289–293.

13 Y. V. Nelyubina, A. S. Shaplov, E. I. Lozinskaya, M. I. Buzin and Y. S. Vygodskii, *J. Am. Chem. Soc.*, 2016, **138**, 10076–10079.

14 J. M. Slattery, C. Daguenet, P. J. Dyson, T. J. S. Schubert and I. Krossing, *Angew. Chem.*, 2007, **119**, 5480–5484; *Angew. Chem., Int. Ed.*, 2007, **46**, 5384–5388.

15 A. Rupp, N. Roznyatovskaya, H. Scherer, W. Beichel, P. Klose, C. Sturm, A. Hoffmann, J. Tübke, T. Koslowski and I. Krossing, *Chem.–Eur. J.*, 2014, **20**, 9794–9804.

16 W. Beichel, Y. Yu, G. Dlubek, R. Krause-Rehberg, J. Pionteck, D. Pfefferkorn, S. Bulut, D. Bejan, C. Friedrich and I. Krossing, *Phys. Chem. Chem. Phys.*, 2013, **15**, 8821–8830.

17 P. Barthen, W. Frank and N. Ignatiev, *Ionics*, 2015, **21**, 149–159.

18 W. Beichel, N. Trapp, C. Hauf, O. Kohler, G. Eickerling, W. Scherer and I. Krossing, *Angew. Chem.*, 2014, **126**, 3207–3210; *Angew. Chem., Int. Ed.*, 2014, **53**, 3143–3146.

19 C. Hardacre, J. D. Holbrey, M. Nieuwenhuyzen and T. G. A. Youngs, *Acc. Chem. Res.*, 2007, **40**, 1146–1155.

20 I. Krossing and J. M. Slattery, *Z. Phys. Chem.*, 2006, **220**, 1343–1359.

21 F. Philippi, D. Rauber, O. Palumbo, K. Goloviznina, J. McDaniel, D. Pugh, S. N. Suarez, C. C. Fraenza, A. Padua, C. W. M. Kay and T. Welton, *Chem. Sci.*, 2022, **13**, 9176–9190.

22 T. Endo, K. Sunada, H. Sumida and Y. Kimura, *Chem. Sci.*, 2022, **13**, 7560–7565.

23 I. Krossing, J. M. Slattery, C. Daguenet, P. J. Dyson, A. Oleinikova and H. Weingärtner, *J. Am. Chem. Soc.*, 2006, **128**, 13427–13434.

24 P. M. Dean, J. M. Pringle and D. MacFarlane, *Phys. Chem. Chem. Phys.*, 2010, **12**, 9144–9153.

25 H. Tokuda, K. Hayamizu, K. Ishii, M. A. B. H. Susan and H. Watanabe, *J. Phys. Chem. B*, 2005, **109**, 6103–6110.

26 S. Tsuzuki, H. Matsumoto, W. Shinoda and K. Mikami, *Phys. Chem. Chem. Phys.*, 2011, **13**, 5987–5993.

27 T. Endo, M. Imanari, H. Seki and K. Nishikawa, *J. Phys. Chem. A*, 2011, **115**, 2999–3005.

28 P. A. Hunt, *J. Phys. Chem. B*, 2007, **111**, 4844–4853.

29 S. Zahn, G. Bruns, J. Thar and B. Kirchner, *Phys. Chem. Chem. Phys.*, 2008, **10**, 6921–6924.

30 P. A. Hunt, C. R. Ashworth and R. P. Matthews, *Chem. Soc. Rev.*, 2015, **44**, 1257–1288.

31 L. K. Scarbath-Evers, P. A. Hunt, B. Kirchner, D. R. MacFarlane and S. Zahn, *Phys. Chem. Chem. Phys.*, 2015, **17**, 20205–20216.

32 M. H. Kowsari and S. Ebrahimi, *Phys. Chem. Chem. Phys.*, 2018, **20**, 13379–13393.

33 J. Foropoulos and D. D. DesMarteau, *Inorg. Chem.*, 1984, **23**, 3720–3723.

34 K. Liu, Z. Wang, L.-X. Shi, S. Jungsuttiwong and S. Yuan, *J. Energy Chem.*, 2021, **59**, 320–333.

35 T. Rüther, A. I. Bhatt, A. S. Best, K. R. Harris and A. F. Hollenkamp, *Batteries Supercaps*, 2020, **3**, 793–827.

36 C. Lian, H. Liu, C. Li and J. Wu, *AIChE J.*, 2019, **65**, 804–810.

37 B. A. Shainyan and L. L. Tolstikova, *Chem. Rev.*, 2013, **113**, 699–733.

38 P. Bonhôte, A.-P. Dias, N. Papageorgiou, K. Kalyanasundaram and M. Grätzel, *Inorg. Chem.*, 1996, **35**, 1168–1178.

39 A. Mauger, C. M. Julie, A. Paolella, M. Armand and K. Zaghib, *Mater. Sci. Eng., R*, 2018, **134**, 1–21.

40 P. Simon and Y. Gogotsi, *Nat. Mater.*, 2008, **7**, 845–854.

41 G. A. Giffin, *J. Mater. Chem. A*, 2016, **4**, 13378–13389.

42 J. Kalhoff, G. G. Eshetu, D. Bresser and S. Passerini, *ChemSusChem*, 2015, **8**, 2154–2175.

43 D. R. MacFarlane, N. Tachikawa, M. Forsyth, J. M. Pringle, P. C. Howlett, G. D. Elliott, J. H. Davis Jr, M. Watanabe, P. Simon and C. A. Angell, *Energy Environ. Sci.*, 2014, **7**, 232–250.

44 M. Armand, F. Endres, D. R. MacFarlane, H. Ohno and B. Scrosati, *Nat. Mater.*, 2009, **8**, 621–629.

45 S. N. Suarez, A. Rúa, D. Cuffari, K. Pilar, J. L. Hatcher, S. Ramati and J. F. Wishart, *J. Phys. Chem. B*, 2015, **119**, 14756–14765.

46 O. Borodin, W. Gorecki, G. D. Smith and M. Armand, *J. Phys. Chem. B*, 2010, **114**, 6786–6798.

47 R. Koshar, EP0057327, Minnesota Mining & Manufacturing Company, 1982.

48 S. Kakinuma, T. Ishida and H. Shirota, *J. Phys. Chem. B*, 2017, **121**, 250–264.

49 B. O'Rourke, C. Lauderback, L. I. Teodoro, M. Grimm, M. Zeller, A. Mirjafari, G. L. Guillet and P. C. Hillesheim, *ACS Omega*, 2021, **6**, 32285–32296.

50 S. Yamaguchi, H. Yamada, Y. Takeoka, M. Rikukawa and M. Yoshizawa-Fujita, *New J. Chem.*, 2019, **43**, 4008–4012.

51 S. Kakinuma and H. Shirota, *J. Phys. Chem. B*, 2019, **123**, 1307–1323.

52 M. Moriya, T. Watanabe, W. Sakamoto and T. Yogo, *RSC Adv.*, 2012, **2**, 8502–8507.

53 M. Moriya, T. Watanabe, S. Nabeno, W. Sakamoto and T. Yogo, *Chem. Lett.*, 2014, **43**, 108–110.

54 J. Traver, E. Chenard, M. Zeller, G. L. Guillet, W. E. Lynch and P. C. Hillesheim, *J. Mol. Struct.*, 2021, **1232**, 130046.

55 R. Jüschke, G. Henkel and P. Sartori, *Z. Naturforsch., B: Chem. Sci.*, 1997, **52**, 359–366.

56 L. Pohl, V. Hilarius, P. Sartori and R. Jüschke, WO97/31909, Merck Patent GmbH, 1997.

57 R. Jüschke, D. Velayutham and P. Sartori, *J. Fluorine Chem.*, 1997, **83**, 145–149.

58 S. Schaltin, N. R. Brooks, L. Stappers, K. Van Hecke, L. Van Meervelt, K. Binnemans and J. Fransaer, *Phys. Chem. Chem. Phys.*, 2012, **14**, 1706–1715.

59 M. Stricker, B. Oelkers, C. P. Rosenau and J. Sundermeyer, *Chem.–Eur. J.*, 2013, **19**, 1042–1057.

60 Y. Tang and B. Yu, *Eur. J. Inorg. Chem.*, 2020, 107–118.

61 A. Blaschette, P. G. Jones, T. Hamann, M. Nävcke, D. Schomburg, H. K. Cammenga, M. Epple and I. Steppuhn, *Z. Anorg. Allg. Chem.*, 1993, **619**, 912–922.

62 Y. U. Paulechka, G. J. Kabo, A. V. Blokhin, A. S. Shaplov, E. I. Lozinskaya, D. G. Golovanov, K. A. Lyssenko, A. A. Korlyukov and Y. S. Vygodskii, *J. Phys. Chem. B*, 2009, **113**, 9538–9546.

63 A. R. Choudhury, N. Winterton, A. Steiner, A. I. Cooper and K. A. Johnson, *CrystEngComm*, 2006, **8**, 742–745.

64 A. R. Choudhury, N. Winterton, A. Steiner, A. I. Cooper and K. A. Johnson, *J. Am. Chem. Soc.*, 2005, **127**, 16792–16793.

65 H. Li, L. Su, X. Cheng, K. Yang and G. Yang, *J. Phys. Chem. B*, 2014, **118**, 8684–8690.

66 L. Su, M. Li, X.-L. Zhu, Z. Wang, Z.-N. Chen, F. Li, Q. Zhou and S. Hong, *J. Phys. Chem. B*, 2010, **114**, 5061–5065.

67 G. R. Desiraju, *J. Am. Chem. Soc.*, 2013, **135**, 9952–9967.

68 A.-V. Mudring, *Aust. J. Chem.*, 2010, **63**, 544–564.

69 R. Hayes, G. G. Warr and R. Atkin, *Chem. Rev.*, 2015, **115**, 6357–6426.

70 C. M. Burba, J. Janzen, E. D. Butson and G. L. Coltrain, *J. Phys. Chem. B*, 2013, **117**, 8814–8820.

71 L. M. Varela, J. Carrete, M. Turmine, E. Rilo and O. Cabeza, *J. Phys. Chem. B*, 2009, **113**, 12500–12505.

72 S. Bouguerra, I. B. Malham, P. L'etellier, A. Mayaffre and M. Turmine, *J. Chem. Thermodyn.*, 2008, **40**, 146–154.

73 M. Finze and G. J. Reiss, *Acta Crystallogr., Sect. E: Struct. Rep. Online*, 2012, **E68**, o1992–o1993.

74 T. Mochida, Y. Funasako, T. Inagaki, M.-L. Li, K. Asahara and D. Kuwahara, *Chem.–Eur. J.*, 2013, **19**, 6257–6264.

75 T. Mochida, M. Ishida, T. Tominaga, K. Takahashi, T. Sakurai and H. Ohta, *Phys. Chem. Chem. Phys.*, 2018, **20**, 3019–3028.

76 D. D. DesMarteau, S. S. Zuberi, W. T. Pennington and B. B. Randolph, *Eur. J. Solid State Inorg. Chem.*, 1992, **29**, 777–789.

77 O. V. Dolomanov, L. J. Bourhis, R. J. Gildea, J. A. K. Howard and H. Puschmann, *J. Appl. Crystallogr.*, 2009, **42**, 339–341.

78 A. L. Spek, *Acta Crystallogr., Sect. C: Cryst. Struct. Commun.*, 2015, **71**, 9–18.

79 A. L. Spek, *PLATON, A Multipurpose Crystallographic Tool*, Utrecht University, Utrecht, The Netherlands, 2010.

80 A. L. Spek, *Acta Crystallogr., Sect. B: Struct. Sci.*, 2009, **D65**, 148–155.

81 F. Capitani, S. Gatto, P. Postorino, O. Palumbo, F. Trequattrini, M. Deutsch, J.-B. Brubach, P. Roy and A. Paolone, *J. Phys. Chem. B*, 2016, **120**, 1312–1318.

82 F. Capitani, F. Trequattrini, O. Palumbo, A. Paolone and P. Postorino, *J. Phys. Chem. B*, 2016, **120**, 2921–2928.

83 W. Beichel, P. Eiden and I. Krossing, *ChemPhysChem*, 2013, **14**, 3221–3226.

84 J. J. McKinnon, M. A. Spackman and A. S. Mitchell, *Acta Crystallogr., Sect. B: Struct. Sci.*, 2004, **60**, 627–668.

85 J. J. McKinnon, D. Jayatilaka and M. A. Spackman, *Chem. Commun.*, 2007, 3814–3816.

86 M. A. Spackman and D. Jayatilaka, *CrystEngComm*, 2009, **11**, 19–32.

87 F. L. Hirshfeld, *Theor. Chim. Acta*, 1977, **44**, 129–138.

88 M. A. Spackman, J. J. McKinnon and D. Jayatilaka, *CrystEngComm*, 2008, **10**, 377–388.

89 B. Burgenmeister, K. Sonnenberg, S. Riedel and I. Krossing, *Chem.–Eur. J.*, 2017, **23**, 11312–11322.

90 P. M. Dean, J. M. Pringle, C. M. Forsyth, J. L. Scott and D. R. MacFarlane, *New J. Chem.*, 2008, **32**, 2121–2126.

91 M. J. Turner, J. J. McKinnon, S. K. Wolff, D. J. Grimwood, P. R. Spackman, D. Jayatilaka and M. A. Spackman, *CrystalExplorer17*, University of Western Australia, 2017.

92 P. R. Spackman, M. J. Turner, J. J. McKinnon, S. K. Wolff, D. J. Grimwood, D. Jayatilaka and M. A. Spackman, *J. Appl. Crystallogr.*, 2021, **54**, 1006–1011.

93 T. Steiner, *Angew. Chem.*, 2002, **114**, 50–80; *Angew. Chem., Int. Ed.*, 2002, **41**, 48–76.

94 I. Geronimo, N. J. Singh and K. S. Kim, *Phys. Chem. Chem. Phys.*, 2011, **13**, 11841–11845.

95 C. J. Dymek, D. A. Grossie, A. V. Fratini and W. W. Adams, *J. Mol. Struct.*, 1989, **213**, 25–34.

96 S. K. Panja, N. Dwivedi, H. Noothalapati, S. Shigeto, A. K. Sikder, A. Saha, S. S. Sunkari and S. Saha, *Phys. Chem. Chem. Phys.*, 2015, **17**, 18167–18177.

97 J. S. Wilkes and M. J. Zaworotko, *Supramol. Chem.*, 1993, **1**, 191–193.

98 I. de Pedro, A. García-Saiz, J. Dupont, P. Migowski, O. Vallcorba, J. Junquera, J. Rius and J. Rodríguez Fernández, *Cryst. Growth Des.*, 2015, **15**, 5207–5212.

99 R. P. Matthews, T. Welton and P. A. Hunt, *Phys. Chem. Chem. Phys.*, 2014, **16**, 3238–3253.

100 R. P. Matthews, T. Welton and P. A. Hunt, *Phys. Chem. Chem. Phys.*, 2015, **17**, 14437–14453.

101 W. Gao, Y. Tian and X. Xuan, *J. Mol. Graphics Modell.*, 2015, **60**, 118–123.

102 H. Weber and B. Kirchner, *J. Phys. Chem. B*, 2016, **120**, 2471–2483.

103 F. Tang, T. Ohto, T. Hasegawa, M. Bonn and Y. Nagata, *Phys. Chem. Chem. Phys.*, 2017, **19**, 2850–2856.

104 Y.-L. Wang, A. Laaksonen and M. D. Fayer, *J. Phys. Chem. B*, 2017, **121**, 7173–7179.

105 Y.-L. Wang, *J. Phys. Chem. B*, 2018, **122**, 6570–6585.

106 Y. K. J. Bejaoui, N. V. Ignat'ev and M. Finze, manuscript in preparation.

107 *Electrochemical Aspects of Ionic Liquids*, ed. H. Ohno, John Wiley & Sons, Inc., Hoboken, New Jersey, USA, 2nd edn, 2011.

108 M. Salanne, *Top. Curr. Chem.*, 2017, **375**, 63.

109 A. Vioux and B. Coasne, *Adv. Energy Mater.*, 2017, **7**, 1700883.

110 Q. Yang, Z. Zhang, X.-G. Sun, Y.-S. Hu, H. Xing and S. Dai, *Chem. Soc. Rev.*, 2018, **47**, 2020–2064.

111 A. Lahiri, N. Borisenko and F. Endres, *Top. Curr. Chem.*, 2018, **376**, 55–83.

112 A. Balducci, *Top. Curr. Chem.*, 2017, **375**, 1–27.

113 L. Yu and G. Z. Chen, *Front. Chem.*, 2019, **7**, 272.

114 A. Basile, M. Hilder, F. Makhlooghiazad, C. Pozo-Gonzalo, D. R. MacFarlane, P. C. Howlett and C. M. Forsyth, *Adv. Energy Mater.*, 2018, **8**, 1703491.

115 M. Forsyth, L. Porcarelli, X. Wang, N. Goujon and D. Mecerreyes, *Acc. Chem. Res.*, 2019, **52**, 686–694.

116 M. Kar, N. V. Plechkova, K. R. Seddon, J. M. Pringle and D. R. MacFarlane, *Aust. J. Chem.*, 2019, **72**, 3–10.

117 C. Dai, J. Zhang, C. Huang and Z. Lei, *Chem. Rev.*, 2017, **117**, 6929–6983.

118 J. P. Hallett and T. Welton, *Chem. Rev.*, 2011, **111**, 3508–3576.

119 Y. Chen and T. Mu, *Green Chem.*, 2019, **21**, 2544–2574.

120 B. Mandal, S. Ghosh and B. Basu, *Top. Curr. Chem.*, 2019, **377**, 30.

121 K. Paduszyński and U. Domańska, *J. Chem. Inf. Model.*, 2014, **54**, 1311–1324.

122 S. Jiang, Y. Hu, Y. Wang and X. Wang, *J. Phys. Chem. Ref. Data*, 2019, **48**, 033101.

123 N. V. Ignat'ev, M. Finze, J. A. P. Sprenger, C. Kerpen, E. Bernhardt and H. Willner, *J. Fluorine Chem.*, 2015, **177**, 46–54.

124 A. Shakeel, H. Mahmood, U. Farooq, Z. Ullah, S. Yasin, T. Iqbal, C. Chassagne and M. Moniruzzaman, *ACS Sustainable Chem. Eng.*, 2019, **7**, 13586–13626.

125 F. Philippi, D. Rauber, K. L. Eliasen, N. Bouscharain, K. Niss, C. W. M. Kay and T. Welton, *Chem. Sci.*, 2022, **13**, 2735–2743.

126 T. Yim, Y. J. Lee, H.-J. Kim, J. Mun, S. Kim, S. M. Oh and Y. G. Kim, *Bull. Korean Chem. Soc.*, 2007, **28**, 1567–1572.

127 T. Belhocine, S. A. Forsyth, H. Q. N. Gunaratne, M. Nieuwenhuyzen, P. Nockemann, A. V. Puga, K. R. Seddon, G. Srinivasan and K. Whiston, *Green Chem.*, 2011, **13**, 3137–3155.

128 D. R. MacFarlane, J. Golding, S. Forsyth, M. Forsyth and G. B. Deacon, *Chem. Commun.*, 2001, 1430–1431.

129 D. R. MacFarlane, S. A. Forsyth, J. Golding and G. B. Deacon, *Green Chem.*, 2002, **4**, 444–448.

130 N. Zec, M. Bešter-Rogač, M. Vraneš and S. Gadžurić, *J. Chem. Thermodyn.*, 2015, **91**, 327–335.

131 G. McHale, C. Hardacre, R. Ge, N. Doy, R. W. K. Allen, J. M. MacInnes, M. R. Bown and M. I. Newton, *Anal. Chem.*, 2008, **80**, 5806–5811.

132 Y. Jin, Y. Shi, W. Zhang, X. Qi, H. Xia and Q. Zhang, *J. Mol. Liq.*, 2021, **336**, 116572.

133 B. Zheng, Y. Zhang, Z. Zhang, L.-S. Long, S. Chen and S. Zhang, *ChemistrySelect*, 2018, **3**, 284–288.

134 J. N. C. Lopes, K. Shimizu, A. A. H. Pádua, Y. Umebayashi, S. Fukuda, K. Fujii and S.-i. Ishiguro, *J. Phys. Chem. B*, 2008, **112**, 1465–1472.

135 J. E. Kilpatrick, K. S. Pitzer and R. Spitzer, *J. Am. Chem. Soc.*, 1947, **69**, 2483–2488.

136 L. Chan, G. M. Morris and G. R. Hutchinson, *J. Chem. Theory Comput.*, 2021, **17**, 2099–2106.

137 L. A. Bischoff, M. Drisch, C. Kerpen, P. T. Hennig, J. Landmann, J. A. P. Sprenger, R. Bertermann, M. Grüne, Q. Yuan, J. Warneke, X.-B. Wang, N. V. Ignat'ev and M. Finze, *Chem.–Eur. J.*, 2019, **25**, 3560–3574.

138 V. Mazan and M. Boltoeva, *J. Mol. Liq.*, 2017, **240**, 74–79.

139 J. R. Sangoro, C. Iacob, S. Naumov, R. Valiullin, H. Rexhausen, J. Hunger, R. Buchner, V. Strehmel, J. Kärger and F. Kremer, *Soft Matter*, 2011, **7**, 1678–1681.